Mon. Not. R. Astron. Soc. **319**, 728–758 (2000)

Infrared colours for Mira-like long-period variables found in the *Hipparcos* Catalogue

Patricia Whitelock,[1]★ Freddy Marang[1] and Michael Feast[2]★
[1]*South African Astronomical Observatory, PO Box 9, Observatory 7935, South Africa*
[2]*Astronomy Department, University of Cape Town, Rondebosch 7701, South Africa*

Accepted 2000 May 30. Received 2000 May 19; in original form 2000 January 17

ABSTRACT

Near-infrared, *JHKL*, photometry is presented for 193 Mira and semi-regular variables that were observed by *Hipparcos*; periods, bolometric magnitudes and amplitudes are derived for 92 of them. Because of the way in which the *Hipparcos* targets were selected, this group of stars provides a useful data base of Miras with low mass-loss rates ($\dot{M} \lesssim 10^{-7}\,\mathrm{M}_{\odot}\,\mathrm{yr}^{-1}$). Various period–colour relationships are discussed in detail. The colour, particularly $K-L$, at a given period is found to depend on the pulsation amplitude of the star. A comparison with models suggests that this is a consequence of atmospheric extension, in the sense that large-amplitude pulsators have very extended atmospheres and redder $K-L$ and $H-K$ but bluer $J-H$ than their lower amplitude counterparts. The stars with very extended atmospheres also have higher values of $K-[12]$ and hence higher mass-loss rates. This finding provides further evidence for the causal connection between pulsation and mass loss. Two sequences are identified in the $Hp-K$ versus $\log P$ diagram (where Hp is the *Hipparcos* broad-band magnitude) at short periods ($\log P < 2.35$). At a given period these two groups have, on average, the same pulsation amplitude, but different *JHKL* colours and spectral types. The short-period stars in the bluer sequence have similar near-infrared colours to the Miras found in globular clusters.

Long-term trends in the infrared light curves are discussed for stars that have sufficient data.

Key words: stars: AGB and post-AGB – stars: variables: other – infrared: stars.

1 INTRODUCTION

Low- and intermediate-mass stars become Mira variables when they reach the top of the asymptotic giant branch (AGB). They will remain in this most luminous phase in their evolution for very roughly 2×10^{5} yr, before crossing the Hertzsprung–Russell diagram, perhaps as planetary nebulae, to seek oblivion as white dwarfs. Detailed study of these stars is of current interest for two broad reasons. First, they are rather poorly understood: the connection between mass loss, which occurs copiously towards the end of the Mira phase, and the physical parameters of the star is uncertain, and even the pulsation mode, fundamental or overtone, remains unclear. Secondly, because of their extreme luminosity and obedience of a period–luminosity relation they have great potential as standard candles among old populations, both for galactic structure studies and as extragalactic distance indicators.

This paper is the first in a series of three (although the second to appear in print) dealing with Mira-like variables in the solar neighbourhood. In the second paper (Whitelock & Feast 2000, henceforth Paper II), *Hipparcos* parallaxes and the calibration of the Mira period–luminosity relation are discussed together with stellar diameters and the problem of the pulsation mode. In the third paper (Feast & Whitelock 2000b, henceforth Paper III, published first) *Hipparcos* proper motions and radial velocities from the literature are used to discuss the kinematics of Mira-like variables. In the present paper we look in detail at the infrared colours of the Miras observed by *Hipparcos*. Particular emphasis is given to differences between various types of Mira which may be important in analysing their parallaxes and kinematics.

★ E-mail: paw@saao.ac.za (PW); mwf@artemisia.ast.uct.ac.za

2 THE STARS SELECTED

The 229 Mira variables observed by *Hipparcos* were initially selected for this study. An additional 24 semi-regular (SR) and two L-type ‘Mira-like’ variables were included in the study; these were selected on the basis of their optical spectra which showed the emission lines characteristic of the shock waves associated with Mira-like pulsation. A few of these SR Mira-like variables

Table 1. Infrared and other data for variables.

Name	HIP	Sp type	Var	P_{GCVS} (day)	P_{HIP}	ΔHp	Hp_0	$\bar{K}_0$ (mag)	[12]	A_V	d (kpc)
Z Peg	8	M6e-M8.5e Tc	M	334	327	4.01	9.65	1.08	−0.50	0.07	0.63
SV And	344	M5e-M7e	M	316	315	3.96	10.03	2.59	0.73	0.16	1.21
SW Scl #	516	M1III	SRC	146	146	1.30	8.60	3.72	2.17	0.00	1.20
RU Oct	703		M	373	366	2.23	11.32	2.67	0.97	0.09	1.41
SS Cas *	781	M3e-M8e	M	140	138	3.00	10.41	3.21	1.82	0.35	
S Scl	1236	M7/M8IIIe	M	362	373	4.50	8.34	0.31	−1.17	0.00	0.47
T Cas	1834	M6-M9.0e	M	444	443	2.16	7.96	−1.06	−2.75	0.21	0.29
R And	1901	S6,6ev	M	409	409			0.00	−2.52	0.12	0.44
T Scl #	2286	K2III:	M	202	205	2.88	10.17	3.74	2.34	0.00	1.51
TU And	2546	M5e	M	316	321	3.52	9.75	2.12	0.59	0.07	0.98
W Cas	4284	C0ev	M	405	399	2.02	9.09	2.48	1.50	0.77	1.38
W Psc #	4652	M2e-M4	M	188	190	2.61	11.88	5.89	4.10	0.07	3.88
X Cas	9057	C0ev	M	422	420	1.44	9.09	2.32	0.90	0.93	1.31
U Per	9306	M5e-M7e	M	320	320	2.36	8.15	0.89	−0.41	0.35	0.56
Y Eri	9767	Me	M	302	299	2.10	10.13	1.79	0.19	0.02	0.82
R Ari #	10576	M3e-M6e	M	186	185	3.61	9.83	3.93	2.78	0.08	1.56
W And	10687	M7:Sev	M	395	397	5.10	9.26	0.54	−1.74	0.20	0.55
o Cet	10826	M5e-M9e	M	331	333	4.39	5.12	−2.45	−5.42	0.01	0.12
R Cet	11350	M4e-M9e	M	166	168	4.25	9.79	2.54	−0.10	0.02	0.76
S Tri	11423	M2e	M	241	253	1.46	10.55	3.77	2.62	0.13	1.74
R For	11582	C8	M	388		3.30	11.13	0.96	−2.07	0.01	0.66
U Cet	11910	M4/M5e	M	234	234	3.88	9.36	2.77	1.39	0.01	1.07
R Tri	12193	M4IIIe-M8e	M	266	266	3.96	7.92	0.95	−0.53	0.13	0.51
T Ari	13092	M6e-M8e	SRA	316	324	1.66	8.08	0.16	−1.12	0.06	0.40
R Hor	13502	M7e	M	407	415	4.48	7.57	−0.93	−3.34	0.02	0.29
T Hor #	14042	M2/M3e	M	217	219	3.29	9.85	3.32	2.04	0.02	1.31
X Cet #	15465	M2e(S)-M6e	M	177	179	2.68	10.34	4.23	2.93	0.04	1.73
Y Per	16126	C0e	M	248	238	0.61	8.73	3.20	2.24	0.41	1.37
RU Per *	16328	M4e	SRB	170	161	0.79	9.63	1.92	0.52	0.24	
RT Eri	16647	M4e	M	370	368	2.60	9.51	0.39	−1.65	0.03	0.49
T Eri	18336	M5/M6IIIe	M	252	251	3.73	9.70	2.42	1.00	0.03	0.96
W Eri	19567	Md	M	376	378	4.04	9.78	1.50	−1.16	0.04	0.83
SY Per	19931	Ce+...	SRA	474	465	1.11	8.34	1.85	0.56	1.11	1.15
RS Eri	20045	M7e	M	296	299	3.05	9.61	1.22	−0.24	0.05	0.62
R Ret *	21252	Md	M	278	275	3.42	9.41	1.74	0.05	0.06	
RX Tau	21600	M6e-M7e	M	331	329	2.12	10.36	1.20	−0.80	0.13	0.66
R Cae	21766	M6e	M	390	397	3.56	9.71	0.59	−1.68	0.05	0.56
R Pic #	22170	K2/K3II:pe	SR	170	164	1.73	7.82	3.45	1.97	0.05	1.18
SU Dor	22256		M	235	232	3.44	11.01	5.09	3.56	0.06	3.13
EP Ori	22535	M10e	M	358		2.89	11.47	4.10	1.86	0.13	2.66
AU Aur	22796	Ce+...	M	400	377	1.46	10.47	2.72	0.80	0.86	1.52
R Ori	23165	C0ev	M	377	379	2.37	10.44	4.08	2.60	0.18	2.73
R Lep	23203	C7,6e	M	427	444	1.65	7.67	−0.11	−2.51	0.08	0.43
T Lep	23636	M6e-M9e	M	368	370	2.89	9.05	0.08	−1.73	0.07	0.43
U Dor	24055	M8IIIe	M	394	396	3.38	9.92	1.17	−1.48	0.07	0.74
S Pic	24126	M7e	M	428	426	4.37	9.30	0.71	−1.94	0.07	0.63
T Pic #	24468	Me	M	200	201	4.04	10.39	4.26	2.90	0.07	1.91
R Aur	24645	M6.5e-M9.5e	M	457	454	3.72	8.56	−0.96	−2.81	0.20	0.31
T Col	24824	M5/M6e	M	225	224	2.79	8.54	1.95	0.27	0.08	0.72
R Oct	25412	Md	M	405	412	4.00	9.28	0.74	−1.10	0.10	0.62
S Ori	25673	M6.5-M9.5e	M	414	415	3.05	8.75	−0.09	−1.62	0.14	0.43
RU Aur	26675	M7-M9e	M	466	517	5.05	11.61	0.97	−1.71	0.55	0.76
S Cam	26753	C0e	SRA	327	326	1.15	8.78	2.64	1.92	0.20	1.28
S Col	27286	M6e-M8	M	325	327	3.22	10.24	1.58	−0.39	0.12	0.78
U Ori	28041	M6e-M9.5e	M	368	367	4.90	8.42	−0.64	−3.23	0.25	0.29
X Aur #	29441	M3e-M7e	M	163	166	2.86	9.65	3.21	1.90	0.27	1.02
V Mon	30326	M5e-M8e	M	340	333	4.20	8.59	1.05	−0.72	0.37	0.63
V Aur	30449	CVIIe+	M	353	349	1.72	9.67	2.80	1.48	0.26	1.44
RV Pup #	32115	M1e	M	187	188	2.96	9.52	3.61	2.45	0.19	1.35
X Gem	32512	M5e-M8e Tc:	M	264	260	3.10	9.18	1.83	0.14	0.29	0.76
X Mon #	33441	M1IIIe-M6ep	SRA	155	144	1.17	7.43	2.81	1.12	0.63	0.82
R Lyn	33824	S3,9e	M	378	374	4.29	9.64	1.50	0.78	0.14	0.83
R Gem	34356	S3,9e	M	369	370	4.31	8.64	1.76	0.55	0.28	0.92
R CMi	34474	C0ev	M	337	330	2.38	8.37	2.54	1.08	0.48	1.24

Table 1 – *continued*

Name	HIP	Sp type	Var	P_{GCVS} (day)	P_{HIP}	ΔHp	Hp_0	$\bar{K}_0$ (mag)	[12]	A_V	d (kpc)
VX Gem	34859	C8e	M	379	381	1.87	9.29	3.12	1.42	0.39	1.76
L_2 Pup *	34922	M5e	SRB	140	140	0.71	4.15	−2.24	−4.57	0.05	
V Gem	35812	M4-M8(S)E	M	274	272	3.31	9.59	2.78	1.46	0.32	1.21
TT Mon	36043	M5e-M8	M	323	322	3.86	9.10	1.98	−0.33	0.57	0.93
VX Aur	36314	M4e-M6	M	322	323	3.07	9.47	1.65	0.36	0.14	0.80
RX Mon	36394	M6e-M9	M	345	344	3.72	10.20	2.58	1.01	0.59	1.29
S Vol	36423	M4e	M	394	393	3.67	10.46	2.48	0.43	0.15	1.35
Z Pup	36669	Md	M	508	551	3.89	9.66	1.26	−1.45	0.84	0.91
S CMi	36675	M6e-M8e	M	332	326	3.85	8.24	0.46	−1.19	0.22	0.47
U CMi	37459	M4e	M	413	405	3.41	9.85	2.59	1.15	0.28	1.46
W Pup *	37893	M2/M3e	M	119	120	3.28	9.20	3.51	1.98	0.42	
SU Pup	38772	S4,2e	M	339	335	5.45	10.69	2.54	0.85	0.50	1.25
AS Pup	39967	M7e-M9	M	324	326	2.59	8.40	0.23	−1.27	0.35	0.42
TV Cnc	40351	M7	M	366		2.48	11.37	4.61	2.01	0.16	3.42
R Cnc	40534	M6e-M9e	M	361	356	3.32	7.82	−0.63	−2.30	0.10	0.30
SV Pup #	40593	M5e	M	166	166	3.78	10.10	3.56	0.54	0.34	1.22
V Cnc	40977	Sevar	M	272	277	4.48	9.48	3.13	1.70	0.11	1.40
T Lyn	41058	N0e	M	406	409	2.07	9.69	2.96	0.85	0.08	1.72
R Pyx	42975	C(R)e	M	363	361	1.70	8.42	2.69	0.68	0.46	1.40
UW Pyx	43123	Ce	LB	423	423	1.50	9.13	2.79	0.56	0.72	1.63
S Hya	43653	M4e-M8.0e	M	256	259	4.08	9.86	2.84	1.64	0.11	1.18
T Hya	43835	M3e-M9:e	M	298	282	3.98	9.37	2.35	1.19	0.16	1.04
W Cnc	44995	M6.5e-M9e	M	393	389	3.90	9.85	1.04	−0.75	0.05	0.69
Y Vel	46502	M8-M9.5e	M	449	451	3.97	9.73	1.13	−1.00	0.72	0.79
R Car	46806	M6/M7pe	M	308	305	4.27	6.43	−1.36	−2.82	0.14	0.19
X Hya	47066	Md	M	301	304	3.73	8.93	0.64	−1.12	0.11	0.48
R LMi	47886	M6.5-M9.0e	M	372	374	3.58	9.10	−0.35	−2.74	0.03	0.35
R Leo	48036	M6e-M9.5e	M	309	311	3.46	6.37	−2.56	−4.40	0.02	0.11
W Sex	48316	C0e	SR	134	200	0.54	8.91	3.50	2.69	0.06	1.02
S LMi	48520	M2.0e-M8.2e	M	233	232	4.37	9.92	3.96	2.18	0.03	1.85
V Leo	49026	M5e	M	273	274	3.90	10.59	3.16	1.27	0.03	1.43
X Ant #	49524	M2	M	161	162	3.41	10.83	5.39	3.99	0.18	2.78
S Car #	49751	M2/M3e	M	149	150	2.79	6.61	1.84	0.59	0.38	0.51
W Vel	50230	M5-M8IIIe	M	394	389	3.62	9.29	0.44	−1.38	0.48	0.52
V Ant	50697	M7IIIe	M	302	301	3.97	9.86	2.09	−0.93	0.20	0.94
X Oct #	51084	M5/M6e	SRA	199	197	2.33	8.30	1.72	0.41	0.14	0.59
S Sex	51791	M2e-M5e	M	264	252	2.72	10.36	3.41		0.04	1.57
R UMa	52546	M3e-M9e	M	301	299	4.18	8.90	1.37	−1.20	0.04	0.67
WX Vel	52887	M5e-M7IIIe	M	411	414	3.72	11.14	1.75	−0.08	0.62	0.99
WW Vel *	52988	M5e	M	187	392	2.77	10.62	2.44	0.57	0.36	
V Hya	53085	C9I	L	530		2.15	7.36	−0.72	−3.78	0.07	0.38
W Leo	53265	M5.5e-M7e	M	385				2.02		0.02	1.07
CI Vel #	53853	M0e	M	142	139	2.38	10.79	6.30	5.18	0.98	3.86
RT Crt	53915	M8	M	342	183			4.49	1.56	0.04	3.08
DN Hya #	57009	Me	M	182	183			5.36	3.55	0.12	2.98
X Cen	57642	Md	M	315	312	3.60	9.16	1.09	−1.34	0.17	0.61
W Cen #	58107	M5e	M	201	203	3.45	9.11	1.90	0.43	0.51	0.65
R Com	58854	M8e	M	362	359	4.35	10.81	2.21	0.44	0.00	1.12
BH Cru	59844	CS	M	421	517	1.71	7.50	1.50	0.62	0.50	0.90
R Crv	60106	Md	M	317	318	4.10	9.61	1.87	0.26	0.05	0.87
XZ Cen	60502	M5III:e	M	290	268	1.95	9.24	1.50	0.34	0.11	0.70
T CVn	61009	M6.5e	M:	290	294	1.41	9.87	2.04	0.84	0.00	0.89
U Cen #	61286	Me	M	220	221	3.53	9.11	3.09	1.82	0.48	1.19
T UMa	61532	M4IIIe-M7e	M	256	258	4.13	9.69	2.94	1.04	0.02	1.24
R Vir *	61667	M3.5-8.5IIIe	M	145	145	3.27	8.48	2.05	0.78	0.01	
S UMa	62126	S1,5ev	M	225	223	3.00	9.40	3.04	2.34	0.02	1.18
RU Vir	62401	C0	M	433	443	1.73	10.89	1.81	−1.96	0.01	1.06
U Vir #	62712	M2e-M8e	M	206	206	3.80	10.26	4.01	2.52	0.01	1.74
V Cru	63175	C0ev	M	376	375	1.84	8.91	2.80	1.64	0.75	1.51
BZ Vir #	63501	M5e	M	150	151	2.15	11.11	5.34	3.19	0.04	2.58
V CVn #	65006	M4e-M6IIIA:e	SRA	191	191	1.13	7.14	1.22	−1.52	0.01	0.46
R Hya	65835	M6/M7e	M	388	384	2.71	5.64	−2.48	−4.14	0.03	0.14
S Vir	66100	M6IIIe-M9.5e	M	375	370	4.25	8.56	0.33	−1.49	0.02	0.48
RV Cen	66466	N3v	M	446	447	1.25	7.49	1.41	−0.01	0.52	0.90

Table 1 – *continued*

Name	HIP	Sp type	Var	P_{GCVS} (day)	P_{HIP}	ΔHp	Hp_0	$\bar{K}_0$ (mag)	[12]	A_V	d (kpc)
T Cen *	66825	M3e	SRA	90	90	1.79	6.75	2.49	1.35	0.10	
RT Cen	67359	M6II:e	M	255	253	1.40	9.62	2.68	1.55	0.14	1.09
R CVn	67410	M5.5e-M9e	M	328	333	3.36	8.62	0.62	−1.19	0.00	0.50
W Hya	67419	M7e	SRA	361	369	2.02	6.30	−3.16	−5.09	0.03	0.09
RX Cen	67626	M5e	M	327	328	4.99	10.78	2.75	0.78	0.14	1.34
RU Hya	69346	M6e-M8.8e	M	331	332	3.81	9.81	1.74	−0.95	0.09	0.85
R Cen	69754	M5e	M	546	531	2.63	6.73	−0.74		0.35	0.38
U UMi	69816	M6e-M8e	M	330	321	2.51	8.89	0.84	−0.64	0.03	0.56
AO Vir	70209	M2e-M4e	M	254	254	2.19	10.38	4.14	2.39	0.02	2.14
RW Lup #	70590	Mb	M	197	199	1.07	9.34	2.49	0.62	0.24	0.84
RS Vir	70669	M6IIIe-M8e	M	353	351	3.71	9.33	1.10	−1.37	0.02	0.66
R Boo #	71490	M3e-M8e	M	223	225	3.82	9.03	2.11	0.68	0.01	0.77
RR Boo #	72300	M2e-M6e	M	194	195	3.70	11.26	5.28	3.44	0.01	3.00
Y Lib	74350	M5e-M8.2e	M	275	276	4.17	10.60	3.28	1.14	0.05	1.52
RT Boo	74802	M6.5-M8e	M	273	265	2.04	10.63	2.56	1.10	0.02	1.08
S CrB	75143	M6e-M8e	M	360	357	4.09	8.50	0.32	−2.05	0.02	0.47
S Lib #	75144	M2	M	192	194	2.32	10.10	4.51	3.48	0.10	2.09
S Ser	75170	M5e-M6e	M	371	376	2.69	9.79	1.76	−0.26	0.02	0.93
RS Lib *	75393	Me	M	217	221	2.58	8.63	−0.08	−1.81	0.08	
S UMi	75847	M6e-M9e	M	331	324	2.61	8.74	0.19	−1.57	0.06	0.42
RU Lib	76152	Md	M	316	312	3.99	10.06	2.28	0.86	0.09	1.05
R Nor	76377	M3e	M	507	510	4.53	8.49	1.22	−0.63	0.55	0.90
BG Ser	77027	M6e-M8e	M	404	404	2.04	9.51	0.39	−1.35	0.05	0.52
T Nor	77058	M5:e	M	240	240	3.93	8.33	2.09	−0.61	0.78	0.80
X CrB	77460	M5e-M7e	M	241	243	3.59	10.83	3.66	1.92	0.03	1.65
V CrB	77501	N2	M	357	358	2.05	8.86	1.58	−1.12	0.03	0.83
R Ser	77615	M5IIIe-M9e	M	356	355	4.54	8.64	0.82	−1.84	0.04	0.58
AH Ser	78307	M2	M	283	285	3.79	12.12	4.93	2.91	0.04	3.31
RR Her	78721	C7.2e	SRB	239	244	1.61	8.88	3.33	2.19	0.04	1.41
RZ Sco #	78746	M1III	M	156	162	1.93	9.44	4.17	1.97	0.18	1.55
Z Sco	78872	M3/M4e	M	343	350	1.78	9.69	1.46	0.11	0.15	0.77
U Ser	78976	M3e-M6e	M	237	236	4.27	10.23	3.52	2.18	0.05	1.53
RU Her	79233	M6e-M9	M	484	497	4.46	9.46	0.36	−1.79	0.04	0.58
U Her	80488	M6.5e-M9.5e	M	406	418	3.88	8.31	−0.29	−2.87	0.05	0.38
V Oph	80550	C	M	297	296	1.54	8.02	1.63	0.30	0.13	0.75
R Dra	81014	M5e-M9IIIe	M	245	245	3.85	9.37	2.22	0.62	0.06	0.86
SS Her *	81026	M0e-M5e	M	107	107	2.68	10.62	5.07	3.41	0.08	
X Ara *	81309	Md	M	175	175	3.85	10.55	2.38	0.27	0.47	
AS Her	81506	M2e	M	269	267	3.44	10.10	1.96	0.40	0.07	0.82
S Her	82516	M4Se-M7.5Se	M	307	306	4.39	9.11	1.29	0.06	0.08	0.66
Z Ara	82695	Md	M	288	294	3.46	10.58	3.00	1.84	0.52	1.38
RS Sco	82833	M6e	M	319	319	4.45	8.00	0.36	−1.53	0.40	0.44
RR Sco	82912	M6IIIe	M	281	274	3.34	7.40	−0.25	−1.83	0.21	0.30
SY Her *	83304	M1e-M6e	M	116	116	3.04	9.83	4.33	2.66	0.08	
UX Oph *	83582	M4e	M	116	116	3.15	10.77	4.78	2.94	0.23	
SZ Ara	84059	Ce(R-Nb)	M	220	217	1.38	9.66	4.37	3.32	0.33	2.15
Z Oph	84763	K3ep-M7.5e	M	348	345	3.80	9.53	3.99	2.42	0.17	2.49
RS Her #	84948	M4e-M8:	M	219	218	3.25	9.66	2.92	1.34	0.10	1.10
VW Oph	85429	M5e	M	285		2.61	11.56	4.77	2.37	0.18	3.09
Z Oct	86836		M	335	346	2.48	10.92	2.70	1.21	0.12	1.33
T Her #	88923	M2.5e-M8e	M	164	163	3.74	9.64	3.21	1.76	0.16	1.03
XZ Her #	89018	M0	M	171	173			7.00	5.18	0.23	6.06
R Pav	89258	Me	M	229	231	3.65	9.40	2.88	1.36	0.18	1.11
W Lyr #	89419	M2e-M8e	M	197	195	3.37	9.49	3.12	2.15	0.15	1.12
RY Oph *	89568	M3e-M6e	M	150	148	3.00	9.73	2.92	1.63	0.37	
AL Dra	90474	M7ea	M	330	335	3.20	11.30	2.96	0.92	0.14	1.48
RV Sgr	90493	M3e	M	315	322	4.44	9.40	1.59	0.23	0.34	0.77
RS Dra	91316	M5e	SRA	282	292	0.61	9.17	1.95	0.77	0.11	0.84
X Oph	91389	K1IIIv comp	M	328	337	2.07	6.89	−1.00	−2.65	0.18	0.24
V733 Sgr *	93293		M	100	100	2.40	11.45	6.54	5.18	0.46	
R Aql	93820	M5e-M9e	M	284	277	3.11	7.16	−0.78	−2.80	0.23	0.24
SS Lyr	94438	M5IIIevar	M	346	355	2.80	10.63	1.73	−0.09	0.23	0.87

Table 1 – *continued*

Name	HIP	Sp type	Var	P_{GCVS} (day)	P_{HIP}	ΔHp	Hp_0	$\bar{K}_0$ (mag)	[12]	A_V	d (kpc)
RW Sgr #	94489	M3III:e	SRA	186		0.61	8.80	3.03	1.31	0.30	1.03
T Sgr	94706	Se	M	394	384	3.92	9.81	1.26	−0.13	0.28	0.77
R Sgr	94738	M2e	M	269	268	4.28	8.85	2.04	0.56	0.26	0.84
SW Tel	95676	Me	M	229	227	4.20	11.58	5.30	4.08	0.13	3.40
RT Aql	96580	M6e-M8e	M	327	324	3.22	9.23	1.09		0.43	0.62
BG Cyg	96647	M7e-M8e	M	288	287	1.19	9.22	1.02	−0.51	0.44	0.55
TT Cyg	96836	C6.4e	SRB	118		0.38	7.25	1.83	0.99	0.32	0.43
RT Cyg #	97068	M2e-M8.8Ibe	M	190	189	3.68	8.89	3.25	1.87	0.33	1.16
χ Cyg	97629	S7,1e:	M	408	402	5.51	7.44	−1.92	−4.09	0.16	0.18
T Pav	97644	Md	M	243	245	4.31	9.62	2.86	1.38	0.10	1.15
RR Sgr	98077	M5e	M	336	345	4.56	8.55	0.69	−1.52	0.11	0.53
RR Aql	98220	M6e-M9	M	394				0.48	−2.50	0.20	0.54
RU Sgr	98334	M4e	M	240	240	3.93	9.31	2.18	0.38	0.10	0.83
BQ Pav *	98447		M	109	109	3.01	11.52	6.57	5.18	0.09	
S Aql #	99503	M3e-M5.5e	SRA	146	146	1.47	9.85	4.28	2.69	0.44	1.55
R Del	99802	M5e-M6e	M	285	288			1.91	0.12	0.27	0.83
RT Sgr	100033	Me	M	306	307	3.99	9.22	1.32	−0.20	0.08	0.66
WX Cyg	100113	C8e:	M	410	399	1.48	9.49	2.17	1.34	1.05	1.20
X Tel	100137	M5e	M	309		2.56	12.15	4.57	2.46	0.08	2.98
U Cyg	100219	Cme	M	463	460	2.18	7.73	1.34	−1.21	0.48	0.89
V865 Aql	100599	M6-M7e	M	367	366			1.59	0.56	0.18	0.85
U Mic	101063	M6e	M	334	333	3.55	10.36	1.84	−0.03	0.07	0.89
R Mic *	101985	M4e	M	138	138	3.58	10.59	3.65	2.29	0.07	
V Cyg	102082	C7.4e	M	421	417	1.91	9.27	0.27	−3.17	0.39	0.51
S Del	102246	M5-M8e	M	277	277	2.18	9.13	2.06	0.85	0.24	0.87
V Aqr	102546	M6e	SRA	244	235	1.13	7.79	0.57	−0.72	0.11	0.40
AM Cyg	102732	M6e	M	370	365	2.42	11.56	1.82	−0.09	0.46	0.95
T Aqr #	102829	M2e-M5.5e	M	202	204	3.17	9.43	3.23	2.09	0.11	1.20
RX Vul	103069	M9e	M	457	466	1.54	10.28	1.03	−0.84	0.27	0.77
R Vul *	104015	M3e-M7e	M	136	136	3.60	9.77	3.22	1.81	0.25	
V Cap	104285	M3/M4e	M	275	276	3.51	11.18	3.47	1.20	0.05	1.66
T Cep	104451	M5.5e-M8.8e	M	388	400	3.45	6.73	−1.71	−3.31	0.12	0.19
T Cap	105498	Md	M	269	266			3.24	1.58	0.05	1.47
S Cep	106583	C6II	M	486	486	1.79	7.28	−0.05	−2.57	0.16	0.49
W Cyg *	106642	M4IIIe-M6e	SRB	131	132	0.62	5.35	−1.39	−2.52	0.09	
RU Cyg	107036	M6e-M8e	SRA	233	234	0.75	7.37	−0.04	−1.95	0.27	0.29
TU Peg	107390	M7-M8e	M	321	330	2.97	9.90	1.09	−0.63	0.09	0.62
RZ Peg	109089	C9e	M	438	435	3.12	9.18	2.82	0.81	0.22	1.70
RS Peg	109610	M6e-M9e	M	415	421	3.14	9.90	1.19		0.08	0.77
X Aqr	110146	S6,3e	M	311	307			2.95	1.21	0.02	1.42
UU Tuc	110451	M4e	M	335	306	3.08	10.88	3.53	0.53	0.03	1.95
RT Aqr	110509	Md	M	246	248	1.46	9.55	2.17	1.04	0.02	0.84
T Gru #	110697	M0e	M	136	136	2.35	9.88	5.23	3.59	0.02	2.29
S Gru	110736	M8III:e	M	401	396	4.38	9.19	0.68	−1.47	0.02	0.60
S Lac	110972	M4e-M8.2e	M	241	239	3.40	9.57	2.48	0.55	0.26	0.96
SS Peg	111385	M6e-M7e	M	424	420	3.94	9.83	1.10	−0.92	0.10	0.75
T Tuc	111946	M5e	M	250	254	3.84	10.07	3.22	1.48	0.03	1.38
SX Peg	112784	S4,9e	M	303	307	3.53	10.01	3.14	2.31	0.07	1.52
RT Oct #	113652	Me	M	180	177	4.22	11.85	5.71	4.28	0.10	3.47
R Peg	114114	M6e-M9e	M	378	380	4.11	8.73	0.51	−1.82	0.04	0.53
V Cas	114515	M5e-M8.5e	M	228	225	3.17	8.57	0.88	−0.70	0.41	0.44
TY And	114757	M5e-M6e	SRB	260		0.79	8.80	1.63	0.73	0.19	0.68
W Peg	115188	M6e-M8e	M	345	346	2.58	8.83	−0.03	−2.03	0.07	0.39
S Peg	115242	M5E-M8.5E	M	319	328	3.48	9.33	1.41	−0.12	0.03	0.71
R Aqr	117054	M4pe	M	386	383	3.82	7.50	−1.02	−4.10	0.01	0.27
R Cas	118188	M6:e...	M	430	431	4.24	7.05	−1.80	−3.99	0.13	0.20

* SP-red and # SP-blue.

may be misclassified Miras (e.g. S Aql, T Ari, S Cam: Mattei et al. 1997); others unquestionably have SR light curves. Nine stars had to be rejected as no infrared data could be found for them, leaving a total of 246 Mira-like variables with K magnitudes. These are listed in Table 1 together with their variability type (Var), pulsation periods from the General Catalogue of Variable Stars (GCVS) (P_{GCVS}: Kholopov et al. 1985) and from the *Hipparcos* catalogue (P_{Hip}), *Hipparcos* amplitude (ΔHp) and mean reddening-corrected magnitude (Hp_0) (see Section 3.1), mean reddening-corrected K magnitude ($\bar{K}_0$), IRAS 12-μm magnitude

Table 2. Near-infrared photometry. This is a sample of the full table, which is presented in its entirety as Supplementary Material in the electronic version of MNRAS.

JD −2440000	*J*	*H*	*K*	*L*
		(mag)		
Z Peg		HIP 8		
2627.0	2.47	1.53	1.13	0.59
2648.0	2.39	1.50	1.08	0.61
2711.0	2.44	1.48	1.10	0.62
2740.0	2.15	1.33	0.91	0.46
2975.0	2.45	1.62	1.24	0.68
3118.0	2.08	1.19	0.84	0.47
5567.5	2.89	1.84	1.34	0.83
SW Scl		HIP 516		
7852.4	4.82	3.92	3.68	3.35
7888.4	4.91	4.02	3.78	3.46
7900.3	4.91	4.03	3.80	3.46
8875.5	4.76	3.87	3.64	3.31
RU Oct		HIP 703		
9351.3	3.98	2.92	2.53	2.22
9581.7	4.14	3.10	2.69	2.24
9665.3	4.03	3.02	2.63	2.24
9947.6	4.23	3.22	2.81	2.36
9993.5	4.24	3.24	2.83	2.40
10017.4	4.11	3.11	2.73	2.34
10032.4	4.05	3.05	2.68	2.29
10083.3	4.05	2.99	2.61	
10255.7	4.26	3.21	2.77	2.37
10295.6	4.21	3.20	2.78	2.35
10361.4	4.10	3.10	2.73	2.34
10399.4	4.05	3.02	2.64	2.30
10716.5	4.17	3.17	2.78	2.39
10756.4	4.08	3.07	2.69	2.33
S Scl		HIP 1236		
2584.5	2.03	1.19	0.71	0.06
2620.5	1.90	1.07	0.66	0.03
2630.5	1.92	1.02	0.63	0.01
2647.5	1.99	1.10	0.70	0.08
2681.5	1.79	0.94	0.58	0.02
2703.5	1.63	0.74	0.39	−0.09
2729.5	1.48	0.55	0.23	−0.19
2771.5	1.35	0.45	0.10	−0.32
2971.5	1.76	0.88	0.44	−0.12
2995.5	1.72	0.88	0.42	−0.14
2999.5	1.80	0.92	0.54	−0.02
3051.5	1.68	0.84	0.48	0.01
3061.5	1.42	0.56	0.19	−0.37
3078.5	1.33	0.42	0.04	−0.41
3108.5	1.25	0.30	−0.06	−0.50
3136.5	1.26	0.35	−0.05	−0.44
3346.6	2.06	1.15	0.66	0.06
3387.6	1.99	1.12	0.66	0.05
3428.5	1.56	0.72	0.36	−0.15
3431.4	1.54	0.70	0.30	−0.18
3432.4	1.57	0.70	0.33	−0.01
3730.6	1.78	0.97	0.53	−0.03
3848.3	1.24	0.27	−0.03	−0.40
3855.3	1.22	0.23	−0.10	−0.45
3859.3	1.24	0.24	−0.09	−0.45
3860.3	1.21	0.25	−0.08	−0.48
3868.3	1.19	0.24	−0.09	−0.50
3881.2	1.23	0.27	−0.10	−0.46
3882.3	1.26	0.28	−0.09	−0.49
4918.4	1.48	0.56	0.18	−0.34
5158.6	1.77	0.89	0.44	−0.17
5199.6	1.72	0.83	0.41	−0.18
5215.5	1.71	0.84	0.43	−0.13
5251.4	1.59	0.68	0.31	−0.26
5570.6	1.92	1.03	0.60	0.05

Table 2 – *continued*

JD −2440000	*J*	*H*	*K*	*L*
		(mag)		
5616.4	1.63	0.77	0.41	−0.14
5924.5	2.10	1.20	0.73	0.08
6644.6	1.82	0.92	0.47	−0.13
6655.6	1.85	0.94	0.49	−0.09
6690.5	1.81	0.94	0.50	−0.10
6694.5	1.83	0.95	0.52	−0.16
6712.4	1.70	0.83	0.43	−0.14
6740.5	1.45	0.55	0.19	−0.30
6750.4	1.42	0.50	0.15	−0.32
6753.4	1.39	0.47	0.13	−0.35
6774.3	1.28	0.35	0.00	−0.45
6783.3	1.31	0.35	0.01	−0.39
6805.3	1.31	0.34	−0.01	−0.37
6984.7	1.91	0.96	0.50	−0.07
7014.6	1.79	0.90	0.46	−0.12
7023.6	1.77	0.90	0.46	−0.14
7033.6	1.78	0.90	0.47	−0.13
7068.5	1.76	0.88	0.46	−0.14
7113.4	1.37	0.46	0.10	−0.36
7125.4	1.27	0.37	0.03	−0.43
7145.3	1.19	0.28	−0.07	−0.53
7178.3	1.28	0.31	−0.04	−0.45
7328.7	2.05	1.06	0.56	0.02
7357.6	2.03	1.09	0.62	0.03
7372.7	2.08	1.13	0.66	0.06
7378.6	2.07	1.14	0.67	0.06
7426.5	1.97	1.08	0.65	0.08
7446.4	1.78	0.92	0.51	0.00
7501.3	1.37	0.42	0.10	−0.29
7532.3	1.32	0.37	0.01	−0.33
7702.7	2.02	1.02	0.51	−0.05
7728.6	1.89	0.95	0.46	−0.12
7736.6	1.84	0.90	0.42	−0.16
7759.6	1.72	0.82	0.38	−0.25
7761.5	1.71	0.82	0.35	−0.26
7777.6	1.69	0.80	0.36	−0.28
7803.4	1.66	0.77	0.34	−0.28
7837.4	1.45	0.54	0.14	−0.44
7857.4	1.32	0.40	0.01	−0.52
7868.3	1.29	0.35	−0.04	−0.52
8066.7	1.97	1.01	0.52	−0.01
8089.6	1.78	0.88	0.42	−0.13
8106.7	1.72	0.83	0.40	−0.16
8198.4	1.59	0.66	0.30	−0.21
8226.4	1.39	0.44	0.10	−0.32
8252.3	1.28	0.32	−0.02	−0.44
8453.7	2.06	1.14	0.65	0.05
8492.5	1.91	1.04	0.58	−0.01
8499.6	1.91	1.02	0.60	0.02
8517.5	1.95	1.06	0.63	0.02
8554.4	1.76	0.87	0.49	−0.07
8579.4	1.55	0.65	0.29	−0.18
8793.7	2.07	1.09	0.57	0.05
8817.7	2.00	1.06	0.57	0.03
8843.6	1.90	1.00	0.53	−0.07
8868.6	1.86	0.95	0.51	−0.03
8896.5	1.83	0.94	0.52	−0.07
8931.4	1.55	0.67	0.30	−0.22
8960.3	1.33	0.40	0.07	−0.41
8987.3	1.22	0.27	−0.08	−0.48
9004.3	1.21	0.25	−0.11	−0.51
9168.7	2.04	1.07	0.58	−0.03
9215.5	1.91	1.00	0.55	−0.06
9232.5	1.89	1.00	0.55	−0.04
9300.4	1.55	0.68	0.33	−0.21
9498.6	2.09	1.08	0.57	0.07
9525.7	2.11	1.12	0.62	0.10
9582.6	1.88	0.90	0.55	−0.01
9609.5	1.93	1.04	0.61	0.05
9637.4	1.92	1.04	0.62	0.05

Table 2 – *continued*

JD −2440000	*J*	*H*	*K*	*L*	
		(mag)			
9675.3	1.56	0.68	0.34	−0.17	
9709.3	1.37	0.44	0.09	−0.32	
9728.3	1.30	0.35	0.01	−0.41	
9936.6	1.91	1.03	0.56	−0.05	
9979.5	1.96	1.08	0.63	0.01	
9986.5	1.99	1.10	0.64	0.05	
10090.3	1.32	0.40	0.04	−0.38	
10111.3	1.34	0.36	0.01	−0.38	
10296.6	2.10	1.14	0.65	0.08	
10361.4	1.92	1.04	0.61	0.06	
10399.5	1.61	0.74	0.36	−0.15	
10437.3	1.31	0.41	0.08	−0.38	
10620.7	2.22	1.21	0.67	0.09	
10673.6	2.00	1.10	0.60	−0.08	
10736.4	1.95	1.09	0.62	−0.08	
10802.2	1.38	0.48	0.12	−0.39	
10830.3	1.22	0.32	−0.04	−0.51	
T Scl		HIP 2286			
7863.4	5.12	4.28	3.97	3.50	
7890.3	5.17	4.27	3.97	3.56	
7893.4	5.12	4.24	3.95	3.54	
10792.3	5.03	4.12	3.86	3.50	
10829.3	4.73	3.82	3.56		
10853.2	4.74	3.81	3.51	3.22	
10974.7	5.14	4.23	3.93	3.50	
11024.7	4.78	3.85	3.59	3.28	
11051.6	4.70	3.81	3.50	3.17	
TU And		HIP 2546			
10793.3	3.53	2.59	2.20	1.71	
11051.6	3.49	2.56	2.14	1.70	
W Psc		HIP 4652			
9356.3	6.91	6.01	5.69	5.34	
10053.3	6.96	6.02	5.69	5.24	
10295.6	6.92	6.01	5.65	5.26	
10320.6	7.22	6.33	5.93	5.44	
10360.5	7.44	6.57	6.14	5.80	:
10414.3	7.28	6.41	6.08	5.52	:
10721.5	7.34	6.47	6.05	5.69	
10796.3	7.13	6.21	5.89	5.38	:
Y Eri		HIP 9767			
9285.5	3.47	2.45	1.99	1.55	
10085.3	2.97	1.97	1.59	1.27	
10120.3	3.01	2.00	1.59	1.22	
10254.7	3.14	2.17	1.79	1.36	
10317.6	2.99	2.01	1.66	1.29	
10359.5	2.95	1.95	1.59	1.24	
10398.5	3.04	2.02	1.63	1.26	
10419.3	3.07	2.05	1.64	1.27	
10420.4	3.07	2.05	1.65	1.28	
10438.3	3.10	2.07	1.65	1.27	
10468.3	3.18	2.15	1.73	1.31	
10716.5	3.19	2.15	1.75	1.38	
10742.5	3.24	2.20	1.78	1.37	
10829.3	3.18	2.22	1.82	1.41	
R Ari		HIP 10576			
2629.5	5.04	4.25	3.96	3.54	
2646.5	4.87	4.12	3.83	3.47	
2710.5	4.96	4.06	3.73	3.26	
2740.5	5.22	4.41	4.00	3.78	
2773.5	5.30	4.35	4.01	3.41	
3008.5	4.89	4.05	3.75	3.29	
3115.5	5.39	4.50	4.14	3.65	
3136.5	5.45	4.58	4.20	3.80	
5567.6	5.39	4.47	4.08	3.62	
5688.3	4.91	4.02	3.67	3.31	

Table 2 – *continued*

JD −2440000	*J*	*H*	*K*	*L*
		(mag)		
10755.4	5.26	4.39	3.99	3.56
10797.3	5.23	4.34	3.96	3.47
o Cet		HIP 10826		
2707.5	−0.45	−1.32	−2.04	−2.74
2728.5	−0.48	−1.36	−2.03	−2.74
2995.5	−1.05	−1.84	−2.36	−2.82
3083.5	−0.89	−1.69	−2.30	−2.89
3108.5	−1.22	−1.96	−2.45	−3.11
3135.5	−1.33	−2.14	−2.58	−3.21
3175.2	−1.74	−2.50	−2.90	−3.41
3347.7	−1.06	−1.99	−2.47	−2.99
3404.5	−1.06	−1.86	−2.37	−2.95
3430.5	−1.08	−1.97	−2.46	−3.08
3524.3	−1.56	−2.50	−2.93	−3.52
4158.5	−1.38	−2.25	−2.65	−3.20
4161.5	−1.22	−2.09	−2.51	−3.12
4904.4	−1.55	−2.45	−2.83	−3.35
5218.5	−1.67	−2.58	−3.01	−3.59
5571.6	−1.65	−2.54	−2.93	−3.51
5923.5	−1.61	−2.49	−2.88	−3.45
7054.5	−0.59	−1.49	−2.08	−2.78
7074.5	−0.66	−1.53	−2.12	−2.85
7114.4	−0.78	−1.66	−2.18	−2.91
7144.3	−1.34	−2.08	−2.51	−3.23
7176.3	−1.54	−2.40	−2.79	−3.33
7191.3	−1.63	−2.48	−2.90	−3.48
7364.7	−0.50	−1.41	−2.01	−2.69
7394.6	−0.38	−1.32	−1.94	−2.69
7427.5	−0.38	−1.31	−1.94	−2.71
7464.4	−1.01	−1.83	−2.31	−3.02
7497.4	−1.35	−2.21	−2.62	−3.15
7534.3	−1.57	−2.44	−2.82	−3.34
7732.6	−0.93	−1.85	−2.37	−2.90
7745.6	−0.95	−1.88	−2.40	−2.99
7761.6	−0.90	−1.85	−2.36	−2.99
7779.5	−1.07	−1.96	−2.45	−3.07
7803.5	−1.38	−2.25	−2.66	−3.19
7821.5	−1.40	−2.33	−2.73	−3.34
7841.4	−1.47	−2.43	−2.82	−3.38
7873.4	−1.62	−2.56	−2.96	−3.42
7905.3	−1.65	−2.58	−2.97	−3.45
8073.7	−0.77	−1.64	−2.16	−2.71
8077.7	−0.78	−1.64	−2.16	−2.76
8086.7	−0.82	−1.67	−2.17	−2.77
8089.7	−0.79	−1.67	−2.16	−2.75
8093.7	−0.80	−1.67	−2.19	−2.79
8104.7	−0.86	−1.70	−2.18	−2.74
8109.6	−0.89	−1.70	−2.18	−2.77
8115.7	−0.91	−1.74	−2.21	−2.79
8119.7	−0.98	−1.78	−2.23	−2.86
8129.6	−1.12	−1.90	−2.33	−2.99
8141.6	−1.19	−2.01	−2.40	−2.97
8160.5	−1.35	−2.20	−2.59	−3.12
8165.5	−1.36	−2.23	−2.60	−3.12
8170.5	−1.40	−2.27	−2.62	−3.10
8172.6	−1.42	−2.30	−2.67	−3.18
8174.6	−1.43	−2.31	−2.69	−3.28
8177.6	−1.46	−2.35	−2.72	−3.22
8211.4	−1.67	−2.54	−2.89	−3.32
8224.4	−1.70	−2.59	−2.94	−3.39
8228.4	−1.72	−2.59	−2.94	−3.36
8234.4	−1.70	−2.59	−2.95	−3.38
8252.4	−1.66	−2.54	−2.92	−3.34
8280.3	−1.55	−2.41	−2.83	−3.23
8285.3	−1.54	−2.41	−2.81	−3.21
8290.3	−1.52	−2.38	−2.80	−3.18
8294.3	−1.51	−2.35	−2.77	−3.19
8297.3	−1.48	−2.35	−2.76	−3.13
8315.2	−1.38	−2.24	−2.65	−3.06

([12]), estimated visual extinction (A_V) and distance (d) in kpc derived from the K period–luminosity relation, $M_K = -3.47 \log P + 0.84$ (Paper II). The periods of two of the Miras, WW Vel and RT Crt, are uncertain (Section 4.1) and they were therefore not used where period information was crucial.

The Miras selected for the *Hipparcos* input catalogue are, of necessity, biased towards visually bright stars; the limiting magnitude was $V \sim 12.4$. An obvious consequence of this is that their dust shells are relatively thin and they are therefore distinctly different from other groups of extreme (high mass-loss rate) AGB stars that have been studied in recent years, e.g. those selected from IRAS or OH maser surveys.

In the following discussion the stars are crudely divided into M-, S- or C-type on the basis of their spectral classifications; the few stars with K-type spectra are always grouped with the M-types and the term 'oxygen-rich' is used collectively for M-, K- and S-types. For this purpose the types listed in the *Hipparcos* catalogue, as given in Table 1, are used; although the SC classification of BH Cru was changed to CS to reflect its current status (Section 4.1) and it is treated as a C-star in the analysis. All M(S) stars are treated as S-types.

3 PHOTOMETRY

3.1 *Hipparcos* photometry

The literature contains very few Miras with good light curve coverage at Johnson V or any of the photoelectric bands, in obvious contrast to other types of variable star. Much of what we know about the visual light curves of the these stars comes from amateur magnitude estimates (e.g. Campbell 1955; Mattei 1983). The *Hipparcos* magnitudes therefore provide a new insight on the behaviour of these stars at visual wavelengths. The response of the *Hipparcos* photometric system is described in Vol. 1 of Perryman et al. (1997). The *Hipparcos* magnitude, Hp, and amplitude, ΔHp, used in the following discussion are those derived from the mean of and difference between maximum and minimum light of the curves that are illustrated in Vol. 12 of Perryman et al. (1997), so that they are comparable to the mean K magnitude (defined later). Note that Hp derived in this way often differs from the median value tabulated in the main *Hipparcos* Catalogue (column H44). For a large-amplitude variable, of course, the mean magnitude will be distinctly different from the mean brightness.

3.2 Infrared photometry

In order to provide as uniform a data set as possible, photometry obtained at the South African Astronomical Observatory (SAAO) (Table 2; the full version is available electronically on *Synergy*) is used in preference to other material whenever the light curve coverage is adequate. The times of the observations are given as Julian Date (JD) from which 244 0000 has been subtracted. Most of the *JHKL* measurements were made with the MkII photometer on the 0.75-m telescope at SAAO, Sutherland. They are on the current SAAO system as defined by Carter (1990). A few measurements were made on the SAAO 1.9-m; these have been transformed to the SAAO system.[1] The post-1979 photometry is accurate to better than ± 0.03 mag at *JHK*, and to better than ± 0.05 mag at L. Measurements marked with a colon are accurate to better than 0.1 mag at L. Some older (pre-1979) measurements were reported by Catchpole et al. (1979).[2] The measurements listed in Table 2 differ slightly from those in Catchpole et al., because they have been corrected to Carter's improved values for the standard stars. These measurements are slightly less accurate than the more modern values, but see Catchpole et al. for details.

Some of the photometry discussed in the present paper has already been tabulated by Whitelock et al. (1994, 1997) or by Lloyd Evans (1997 – V Hya) and is not repeated here. A small number of measurements were made at SAAO as part of other programmes by T. Lloyd Evans (for R Ori, R Pyx, W Sex, V Hya, SZ Ara and UU Tuc) and by S. Bagnulo and I. Short (for U Dor, S Pic, L_2 Pup, SU Pup, V Hya, R Hya, RV Cen and W Hya); these are used in the means quoted and in the diagrams, but the basic data will be published elsewhere.

Table 1 lists the K magnitude used in the parallax analysis. Where at least four SAAO measurements are available, K is calculated from the mean of the maximum and minimum magnitudes; exceptions to this are U Ori and RU Hya, where small corrections were applied to take into account the fact that the minima of the light curves have not been observed, and W Vel where the maximum was not observed (while undoubtably some other K magnitudes should also be corrected, the available data are inadequate to estimate properly the values of other corrections, therefore no other changes were made). For those stars for which SAAO observations are not available, K magnitudes taken from Yudin (private communication) or from the literature (Gezari, Pitts & Schmitz 1997) are used in the analysis of the *Hipparcos* parallaxes. These data are not used in the discussions of variability or colour.

Many of the C-star light curves are extremely erratic owing to occasional dust obscuration phases (Whitelock et al. 1997). Treating all the data together confuses the analysis for period, amplitude, etc. For this reason only bright cycles were considered in the analysis of the C-stars, R For, R Lep and V Hya. In a similar way the faint periods of the symbiotic Mira, R Aqr (see Whitelock 1999), were not included in the current analysis. Observations made in these faint phases are included in Table 2, but are marked with an asterisk in the last column to indicate that they are not included in the analysis.

Odd individual measurements for a number of stars were omitted from the analysis, although they are listed in Table 2 where they are marked with asterisks. These measurements are discrepant with the others listed. In some cases this is because they were obtained at a very different time from the other measurements and the behaviour of the star was distinctly different. In other cases the cause of the discrepancy is unclear and it is possible that the observations should be totally rejected.

The following nine Mira-like variables were observed by *Hipparcos* but have no infrared photometry and are therefore not discussed here: X Cam, RS Aur, W Lyn, S Boo, HO Lyr, DD Cyg, CN Cyg, DH Lac and TV And.

Table 3 contains a summary of the information in Table 2, including *JHKL* magnitudes derived from the mean of the two dates corresponding to maximum and minimum K light. The total number of dates on which the star was observed (no.) and the peak-to-peak K amplitude (δK) are also given. If the number of observations is small then δK obviously provides only a lower limit to the true range of the star.

[1] Transformation from the 1.9-m natural system to the SAAO system defined by Carter (1990) assumes that $K_{1.9} = K$ and $(J-H)_{1.9} = 0.95(J-H)$ or $(J-K)_{1.9} = 0.955(J-K)$.

[2] Note that the photometry for S Aql published by Catchpole et al. should probably have been attributed to RS Aql and is not used here.

Table 3. Mean SAAO IR photometry.

Name	*J*	*H*	*K* (mag)	*L*	δK	no.	HIP
Z Peg	2.48	1.51	1.09	0.65	0.50	7	8
SW Scl	4.84	3.95	3.72	3.39	0.15	4	516
RU Oct	4.11	3.08	2.68	2.31	0.30	14	703
S Scl	1.65	0.72	0.31	−0.21	0.84	122	1236
T Scl	4.94	4.04	3.74	3.37	0.47	9	2286
TU And	3.51	2.58	2.17	1.70	0.07	2	2546
W Psc	7.18	6.29	5.90	5.53	0.49	8	4652
Y Eri	3.22	2.21	1.79	1.41	0.41	14	9767
R Ari	5.18	4.30	3.94	3.56	0.53	12	10576
o Cet	−1.04	−1.97	−2.45	−3.10	1.23	104	10826
R Cet	3.88	3.02	2.54	1.90	0.94	30	11350
S Tri	5.11	4.13	3.79	3.45	0.02	2	11423
R For	3.70	2.12	0.96	−0.23	0.80	23	11582
U Cet	3.99	3.15	2.77	2.21	0.88	25	11910
R Tri	2.33	1.40	0.97	0.50	0.68	13	12193
T Ari	1.52	0.52	0.17	−0.15	0.30	23	13092
R Hor	0.46	−0.46	−0.93	−1.53	1.09	52	13502
T Hor	4.58	3.68	3.32	2.91	0.51	14	14042
X Cet	5.45	4.52	4.23	3.87	0.54	15	15465
RT Eri	1.99	0.90	0.39	−0.22	0.43	5	16647
T Eri	3.68	2.80	2.42	1.99	0.69	23	18336
W Eri	3.02	2.06	1.51	0.88	1.09	16	19567
RS Eri	2.52	1.58	1.17	0.66	0.32	4	20045
R Ret	3.12	2.19	1.74	1.23	0.76	22	21252
RX Tau	2.79	1.71	1.21	0.69	0.56	10	21600
R Cae	2.17	1.16	0.59	0.00	1.09	116	21766
R Pic	4.37	3.70	3.45	3.05	0.66	9	22170
SU Dor	6.34	5.50	5.09	4.52	0.90	11	22256
EP Ori	5.40	4.41	3.95	3.48	0.48	3	22535
R Ori	5.87	4.69	4.10	3.65	0.80	14	23165
R Lep	2.12	0.80	−0.10	−0.99	0.64	19	23203
T Lep	1.61	0.58	0.09	−0.46	0.71	16	23636
U Dor	2.96	1.89	1.17	0.38	1.10	35	24055
S Pic	2.36	1.30	0.72	0.03	1.18	93	24126
T Pic	5.46	4.60	4.26	3.79	0.75	14	24468
T Col	3.21	2.34	1.96	1.49	0.76	14	24824
R Oct	2.23	1.26	0.75	0.24	0.60	6	25412
S Ori	1.50	0.41	−0.07	−0.55	0.60	101	25673
S Col	3.06	2.09	1.59	1.00	0.63	12	27286
U Ori	0.72	−0.24	−0.75	−1.41	0.84	56	28041
V Mon	2.42	1.55	1.08	0.51	0.89	20	30326
RV Pup	4.78	3.92	3.63	3.20	0.83	17	32115
X Gem	3.40	2.39	1.92	1.50	0.05	3	32512
X Mon	3.96	3.16	2.87	2.44	0.53	20	33441
R Gem	3.13	2.05	1.67	1.20	0.46	4	34356
R CMi	4.12	3.04	2.58	2.25	0.67	11	34474
VX Gem	5.04	3.80	3.15	2.77	0.68	9	34859
L_2 Pup	−0.88	−1.79	−2.24	−2.87	0.59	71	34922
V Gem	4.08	3.21	2.81	2.42	0.68	9	35812
TT Mon	3.34	2.50	2.05	1.36	0.45	2	36043
RX Mon	3.81	2.84	2.46	1.97	0.31	3	36394
S Vol	4.08	3.00	2.49	1.92	0.02	2	36423
Z Pup	3.22	1.99	1.33	0.57	1.10	72	36669
S CMi	1.83	0.90	0.48	−0.04	0.56	11	36675
U CMi	3.90	2.88	2.61	2.33	0.30	9	37459
W Pup	4.69	3.88	3.54	3.06	0.67	20	37893
SU Pup	3.85	2.98	2.58	2.10	0.80	11	38772
AS Pup	1.60	0.65	0.27	−0.22	0.34	6	39967
TV Cnc	6.02	5.14	4.63	3.99	0.70	2	40351
R Cnc	0.93	−0.10	−0.62	−1.13	0.84	19	40534
SV Pup	4.91	4.05	3.59	2.94	0.68	4	40593
V Cnc	4.46	3.48	3.14	2.69	0.82	25	40977
R Pyx	4.95	3.58	2.73	1.88	0.51	15	42975
UW Pyx	5.01	3.59	2.79	1.99	0.50	4	43123

Table 3 – *continued*

Name	*J*	*H*	*K* (mag)	*L*	δK	no.	HIP
S Hya	4.04	3.16	2.85	2.38	0.64	11	43653
T Hya	3.62	2.69	2.36	1.95	0.48	14	43835
W Cnc	2.28	1.49	1.04	0.60	0.44	5	44995
Y Vel	2.99	1.82	1.19	0.44	1.14	73	46502
R Car	−0.01	−0.93	−1.35	−1.81	0.77	74	46806
X Hya	2.17	1.12	0.65	0.10	0.51	13	47066
R LMi	1.46	0.27	−0.34	−0.91	0.55	10	47886
R Leo	−0.99	−2.03	−2.55	−3.13	0.74	53	48036
W Sex	5.16	3.98	3.51	3.05	0.01	2	48316
V Leo	4.57	3.62	3.17	2.65	0.45	6	49026
X Ant	6.65	5.81	5.41	4.80	0.55	6	49524
S Car	2.93	2.13	1.87	1.44	0.88	34	49751
W Vel	2.08	1.08	0.56	−0.13	0.87	13	50230
V Ant	3.64	2.69	2.10	1.37	0.60	9	50697
X Oct	3.02	2.11	1.73	1.26	0.10	2	51084
S Sex	4.79	3.77	3.42	2.97	0.55	12	51791
WX Vel	3.54	2.42	1.81	1.17	0.70	8	52887
WW Vel	3.95	2.96	2.47	1.86	0.14	4	52988
V Hya	1.75	0.24	−0.71	−1.90	0.49	30	53085
W Leo	3.52	2.52	2.02	1.35	0.76	10	53265
CI Vel	7.60	6.76	6.38	5.88	0.78	7	53853
RT Crt	5.81	4.97	4.49	3.80	0.71	3	53915
DN Hya	6.63	5.76	5.37	4.83	0.56	5	57009
X Cen	2.51	1.64	1.10	0.46	0.61	14	57642
W Cen	3.31	2.38	1.95	1.48	0.66	17	58107
R Com	3.54	2.60	2.21	1.78	0.32	8	58854
BH Cru	3.38	2.16	1.55	1.27	0.79	54	59844
R Crv	3.20	2.28	1.88	1.43	0.73	19	60106
XZ Cen	2.84	1.86	1.51	1.15	0.28	4	60502
T CVn	3.37	2.39	2.04	1.74	0.17	6	61009
U Cen	4.45	3.52	3.13	2.64	0.58	8	61286
R Vir	3.21	2.37	2.05	1.60	0.68	10	61667
RU Vir	4.96	3.11	1.81	0.27	1.08	30	62401
U Vir	5.25	4.41	4.01	3.60	0.33	7	62712
V Cru	4.53	3.34	2.86	2.45	0.70	64	63175
BZ Vir	6.69	5.77	5.35	4.81	0.14	4	63501
R Hya	−1.06	−2.06	−2.47	−2.91	0.57	53	65835
S Vir	1.74	0.80	0.33	−0.20	0.68	13	66100
RV Cen	3.27	2.07	1.45	0.96	0.55	60	66466
T Cen	3.45	2.73	2.50	2.12	0.86	27	66825
RT Cen	3.99	3.03	2.69	2.33	0.22	18	67359
W Hya	−1.63	−2.70	−3.16	−3.64	0.56	24	67419
RX Cen	4.11	3.23	2.77	2.23	0.69	16	67626
RU Hya	2.83	1.98	1.57	1.13	0.50	15	69346
R Cen	0.66	−0.34	−0.70	−1.11	0.35	66	69754
AO Vir	5.41	4.53	4.14	3.59	0.30	3	70209
RW Lup	3.58	2.85	2.52	1.88	0.55	9	70590
RS Vir	2.48	1.62	1.10	0.46	0.91	30	70669
R Boo	3.44	2.52	2.11	1.55	0.70	6	71490
Y Lib	4.55	3.71	3.29	2.72	0.99	15	74350
S CrB	1.68	0.74	0.21	−0.33	0.43	4	75143
S Lib	5.79	4.76	4.51	4.17	0.55	14	75144
S Ser	3.23	2.30	1.80	1.18	0.40	4	75170
RS Lib	1.41	0.41	−0.07	−0.58	0.48	35	75393
RU Lib	3.64	2.70	2.29	1.83	0.73	11	76152
R Nor	2.75	1.64	1.27	0.86	0.61	55	76377
BG Ser	2.13	1.00	0.50	0.08	0.10	3	77027
T Nor	3.57	2.63	2.16	1.61	0.71	6	77058
R Ser	2.27	1.35	0.82	0.18	0.60	5	77615
AH Ser	6.39	5.44	4.93	4.44	0.45	2	78307
RZ Sco	5.39	4.57	4.19	3.73	0.66	15	78746
Z Sco	2.83	1.86	1.48	1.13	0.39	15	78872
U Ser	4.78	3.92	3.52	3.02	0.65	4	78976
RU Her	2.04	0.85	0.28	−0.23	0.54	4	79233

Table 3 – *continued*

Name	*J*	*H*	*K* (mag)	*L*	δK	no.	HIP
U Her	1.24	0.23	−0.29	−0.91	0.75	20	80488
V Oph	3.71	2.40	1.65	1.02	0.53	11	80550
SS Her	6.23	5.49	5.08	4.70	0.64	8	81026
X Ara	3.93	2.92	2.42	1.83	0.65	6	81309
AS Her	3.25	2.27	1.91	1.52	0.00	1	81506
S Her	2.50	1.61	1.30	0.94	0.48	5	82516
Z Ara	4.42	3.44	3.04	2.61	0.29	3	82695
RS Sco	1.75	0.88	0.40	−0.13	0.82	13	82833
RR Sco	1.19	0.22	−0.23	−0.71	0.75	54	82912
SY Her	5.46	4.63	4.33	3.96	0.60	7	83304
UX Oph	6.26	5.27	4.80	4.30	0.00	2	83582
SZ Ara	5.92	4.86	4.40	4.16	0.45	8	84059
Z Oph	5.06	4.28	4.01	3.54	0.66	5	84763
RS Her	4.21	3.31	2.92	2.53	0.35	4	84948
VW Oph	6.23	5.32	4.79	4.22	0.15	2	85429
Z Oct	4.23	3.15	2.71	2.29	0.00	1	86836
T Her	4.46	3.67	3.35	2.91	0.42	3	88923
XZ Her	8.23	7.39	7.04		0.21	2	89018
R Pav	4.21	3.31	2.90	2.38	0.99	12	89258
RY Oph	4.30	3.31	2.96	2.48	0.49	8	89568
RV Sgr	2.97	2.02	1.63	1.15	0.45	18	90493
X Oph	0.40	−0.57	−0.98	−1.42	0.65	29	91389
V733 Sgr	7.73	6.87	6.58	6.11	0.18	3	93293
R Aql	0.67	−0.30	−0.76	−1.21	0.79	45	93820
RW Sgr	4.33	3.42	3.06	2.68	0.23	9	94489
T Sgr	2.87	1.75	1.29	0.74	0.81	23	94706
R Sgr	3.34	2.40	2.06	1.62	0.82	13	94738
SW Tel	6.57	5.68	5.31	4.80	0.40	3	95676
RT Aql	2.52	1.60	1.13	0.51	0.63	9	96580
BG Cyg	2.52	1.50	1.06	0.66	0.06	3	96647
χ Cyg	−0.15	−1.31	−1.91	−2.71	0.81	11	97629
T Pav	4.21	3.33	2.87	2.36	0.76	9	97644

Table 3 – *continued*

Name	*J*	*H*	*K* (mag)	*L*	δK	no.	HIP
RR Sgr	2.00	1.14	0.69	0.16	0.89	14	98077
RR Aql	2.17	1.11	0.50	−0.18	1.10	29	98220
RU Sgr	3.41	2.57	2.18	1.64	0.70	5	98334
BQ Pav	7.66	6.87	6.58	6.10	0.65	16	98447
R Del	3.35	2.41	1.93	1.35	0.71	5	99802
RT Sgr	2.71	1.75	1.33	0.87	0.59	7	100033
X Tel	6.13	5.16	4.58	3.98	0.61	8	100137
V865 Aql	2.98	1.96	1.60	1.27	0.32	7	100599
U Mic	3.25	2.35	1.84	1.27	0.84	21	101063
R Mic	4.96	4.05	3.66	3.22	0.57	7	101985
S Del	3.40	2.42	2.08	1.74	0.38	4	102246
V Aqr	1.90	0.92	0.58	0.25	0.11	3	102546
AM Cyg	3.48	2.43	1.88	1.28	0.11	2	102732
T Aqr	4.61	3.64	3.24	2.74	0.50	14	102829
RX Vul	2.59	1.49	1.06	0.67	0.20	2	103069
R Vul	4.56	3.65	3.24	2.76	0.33	2	104015
V Cap	4.85	3.97	3.48	2.81	0.83	11	104285
T Cap	4.58	3.66	3.24	2.69	0.65	18	105498
TU Peg	2.52	1.53	1.10	0.64	0.13	4	107390
RS Peg	2.86	1.76	1.20	0.57	0.86	7	109610
X Aqr	4.18	3.33	2.96	2.47	0.77	18	110146
UU Tuc	5.07	4.13	3.53	2.79	1.26	66	110451
RT Aqr	3.48	2.52	2.17	1.89	0.23	20	110509
T Gru	6.33	5.54	5.24	4.70	0.79	14	110697
S Gru	2.02	1.13	0.68	0.07	0.98	14	110736
SS Peg	2.71	1.72	1.21	0.54	0.04	3	111385
T Tuc	4.45	3.57	3.22	2.78	0.67	7	111946
SX Peg	4.50	3.46	3.15	2.79	0.68	7	112784
RT Oct	7.02	6.05	5.72	5.28	0.30	3	113652
R Peg	2.25	1.08	0.52	−0.05	0.61	10	114114
W Peg	1.55	0.50	−0.02	−0.54	0.55	6	115188
S Peg	2.78	1.83	1.42	1.02	0.59	12	115242
R Aqr	0.60	−0.46	−1.02	−1.85	1.08	104	117054

3.3 Interstellar extinction

Interstellar extinction corrections, A_V, derived from the Galactic extinction law described by Feast, Whitelock & Carter (1990), were used to correct the observed magnitudes; these are listed in Table 1. Clearly this kind of statistical approach can lead to errors in individual corrections, but the derived extinctions are small, $A_V \lesssim 1.1$ mag, and thus the infrared corrections are very small, $A_K \lesssim 0.1$ mag.

The appropriate way of correcting the *Hipparcos* magnitude, *Hp*, for interstellar extinction is unknown for these very red stars. For the purpose of plotting reddening-corrected colours we assume that $A_{Hp} = 0.9A_V$. None of our conclusions is sensitive to this assumption.

3.4 Bolometric magnitudes

Bolometric magnitudes were calculated by fitting blackbody curves as a function of frequency (Robertson & Feast 1981) to individual sets of *JHKL* measurements. The blackbody fitting technique does not work well if a significant fraction of the flux is reprocessed by circumstellar dust, when account must be taken of the flux at longer wavelengths, but should be perfectly adequate for these optically selected stars.

Bolometric corrections were determined for multiply observed stars, and these are discussed in Section 6.3.

4 VARIABILITY

4.1 Pulsation periods

Periods were determined by the *Hipparcos* team for most of the variables. These periods are shown plotted against the GCVS periods [for a few stars the revised periods of Lysacht (1989a,b,c) are used in place of the GCVS values] in Fig. 1. Mira periods are notoriously erratic, so some differences are to be expected between different determinations. In fact the GCVS and *Hipparcos* determinations agree to better than 10 per cent for all but two of the oxygen-rich stars, RT Crt and WW Vel, and two carbon stars, W Sex and BH Cru. The period of BH Cru is actually thought to have lengthened in recent times (Bateson, McIntosh & Venimore 1988; Walker, Ives & Williams 1995; Bedding, Conn & Zijlstra 2000); at the same time its carbon enrichment has increased (Lloyd Evans 1985). These changes are thought to be the consequences of a helium shell flash, as are the slowly decreasing periods of R Hya and R Aql. In general the GCVS period is adopted in the following discussion.

Periods (P_K) were also determined from a Fourier transform of the *K* light curve for all of the stars with SAAO near-infrared observations on 10 or more dates; these are listed in Table 4. Fig. 2 illustrates the *K* light curves plotted as a function of phase for the O-rich stars. From this it can be seen that the accuracy of the derived periods and amplitudes varies considerably from one star to the next, depending on the the number of observations, their

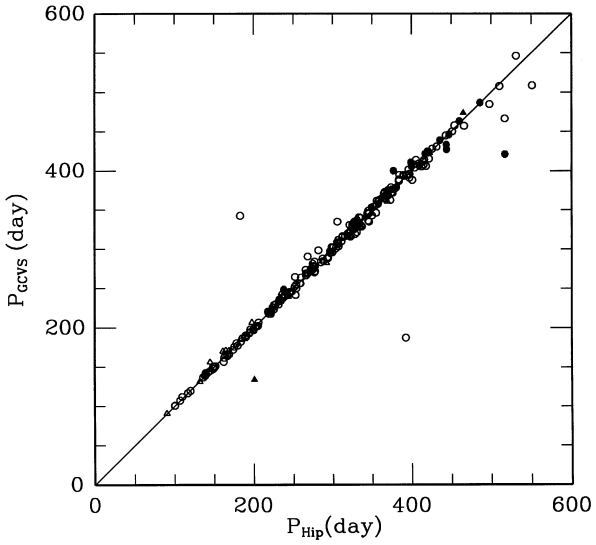

Figure 1. The pulsation period tabulated in the GCVS, P_{GCVS}, is plotted against that determined from the *Hipparcos* data, P_{Hip}. The Miras are shown as circles and the other variables as triangles; oxygen-rich stars are shown as open symbols while carbon stars are closed symbols. The discrepant points are discussed in Section 4.1.

distribution in time and the stability of the light curve over the sampling interval. Most of the illustrations show the K magnitude phased at the period determined from the K data. Exceptions to this are R Ari, T Col, S Col, S CMi and R Pic for which satisfactory periods could not be determined and these are shown phased at the GCVS period. Most of the periods derived in this way are in good agreement with the GCVS values. For three stars, W Leo, Y Lib and X Mon, the period derived from the K light curve differs from the GCVS value by more than 10 per cent. We assume this is a consequence of insufficient K data; for stars with more than 20 observations the K and GCVS periods agree to 3 per cent or better.

4.2 Amplitudes

The definition of the *Hipparcos* amplitude, ΔHp, was given in Section 3.1. Note that eight stars had only lower limits for their *Hipparcos* magnitude at minimum light and they, like the two stars with no maximum or minimum are omitted from this discussion. Fig. 3 is a histogram of the amplitudes for the Miras. It can be compared with similar diagrams discussed by Payne-Gaposchkin (1954) and Whitelock (1997). The Hp amplitudes of the Miras are rather smaller than the V amplitudes tabulated in the GCVS (note that for many stars the GCVS quotes the photographic amplitude or that at some other wavelength). This is probably the result of two factors. First, the very broad response function of the Hp band, with considerable red sensitivity, will result in a somewhat longer effective wavelength than V for these very red stars. Secondly, as a rule the GCVS tabulates the brightest maximum and faintest minimum ever observed for each individual variable. Given that the mean light of Miras tends to vary on a long time-scale, this will inevitably result in a large GCVS amplitude for any star which has been well observed over many years.

The oxygen-rich Miras typically have larger amplitudes than do any of the other groups. Six Miras have $\Delta Hp < 1.5$ mag : S Tri, T CVn, RT Cen, BG Cyg, RT Aqr and RW Lup. Of these, T CVn is actually classified as M: by the GCVS. It has a very erratic light curve and should probably be grouped with the SRs (Koen & Lombard 1995). Similarly, Mattei et al. (1997) suggest that S Tri should be classed as SRa, on the basis of its visual light curve.

The *Hipparcos* amplitudes are shown in Fig. 4 as a function of the period. The SRs in general have lower amplitudes than the Miras (as one would expect from their respective definitions) and there is a slight tendency for longer period stars to have larger amplitudes, although the correlation is very weak. Note that the three largest amplitude stars all have S-type spectra. Similar trends can be seen in fig. 2 of Mennessier, Boughaleb & Mattei (1997).

For stars for which there are 10 or more SAAO IR observations the K amplitudes, ΔK, and bolometric amplitudes, Δm_{bol}, were calculated by fitting a sine wave to the data and measuring the separation of maximum and minimum magnitude; the results are listed in Table 4. A first-order curve was used for most stars because in general it is quite adequate, and in any case rather few stars have sufficient data to establish higher order terms. However, three stars are clearly much better fitted with second- or third-order curves. These are the double-period Miras R Cen and R Nor and the SR variable W Hya. The data for R Cen and W Hya were fitted with second-order curves, while a third-order curve was used for R Nor.

As mentioned above, it is well known that the mean light of Miras quite commonly varies over long periods of time. Changes in the visual amplitude have also been noted for many stars and have recently been discussed by Percy & Bagby (1999) who suggest that some Miras may be double-mode pulsators. Multiple periods and erratic variations are even more common among SR variables. Variations in the infrared mean light and in the amplitude are evident in several of the well observed light curves in Fig. 2. Large variations are particularly clear in the magnitude at minimum of UU Tuc.

Fig. 5 shows a plot of Δm_{bol} against ΔK. The line is a maximum-likelihood fit to the M star data assuming all amplitudes are accurate to ± 0.05 mag:

$$\Delta m_{bol} = 1.210\Delta K - 0.009.$$

The standard deviation of this fit is 0.049 mag. The four SRs fit the relation established for the M-type Miras. The six S stars show a larger K amplitude than do M-type Miras with the same bolometric amplitude.

The K amplitudes are plotted against the Hp amplitudes in Fig. 6. A maximum likelihood fit to the M-type Miras yields

$$\Delta K = 0.16\Delta Hp + 0.06,$$

assuming an uncertainty of 0.05 mag on the measured amplitudes. The standard error on this fit is large, 0.16 mag. There are probably a number of stars with limited IR data for which the K amplitudes are poorly defined. There will also be stars with light curves that are better fitted with sine curves of order two or more. Nevertheless, much of the scatter seen in Fig. 6 must be real.

Fig. 7 shows how the Hp and K amplitudes depend on period for sources with at least 10 IR measurements. While there are more long-period variables with large amplitudes, the correlation is clearly rather weak.

5 $H_P - K$ COLOUR

The colour $(Hp - K)_0$ is constructed using the mean Hp and K magnitudes (Table 1). A plot of this colour against period is shown

Table 4. Fourier Mean SAAO IR photometry.

Name	P_K (day)	$(J-H)_0$	$(H-K)_0$	$(K-L)_0$	K_0 (mag)	m_{bol}	ΔK	Δm_{bol}	HIP
RU Oct	373	1.04	0.41	0.36	2.66	5.78	0.24	0.24	703
S Scl	366	0.95	0.42	0.49	0.27	3.35	0.67	0.75	1236
Y Eri	303	0.99	0.39	0.39	1.73	4.79	0.31	0.27	9767
R Ari		0.84	0.33	0.42	3.89	6.81	0.45	0.58	10576
o Cet	334	0.87	0.46	0.56	−2.54	0.56	0.84	1.01	10826
R Cet	166	0.85	0.47	0.62	2.57	5.68	0.80	0.94	11350
U Cet	236	0.83	0.39	0.51	2.78	5.78	0.71	0.85	11910
R Tri	264	0.90	0.41	0.47	0.91	3.99	0.61	0.77	12193
T Ari	321	0.99	0.36	0.34	0.21	3.26	0.23	0.22	13092
R Hor	402	0.92	0.48	0.58	−0.97	2.17	0.70	0.80	13502
T Hor	214	0.89	0.34	0.42	3.34	6.30	0.48	0.56	14042
X Cet	176	0.94	0.28	0.35	4.19	7.13	0.44	0.48	15465
T Eri	257	0.90	0.37	0.44	2.45	5.47	0.49	0.54	18336
W Eri	378	0.95	0.52	0.59	1.49	4.67	0.97	1.20	19567
R Ret	277	0.86	0.42	0.48	1.80	4.85	0.69	0.78	21252
RX Tau	333	1.03	0.50	0.53	1.22	4.42	0.55	0.69	21600
R Cae	397	1.02	0.53	0.64	0.69	3.91	0.78	0.95	21766
SU Dor	230	0.81	0.40	0.52	5.10	8.11	0.76	0.96	22256
T Lep	362	0.98	0.48	0.54	0.12	3.28	0.65	0.85	23636
U Dor	399	0.97	0.60	0.71	1.14	4.39	0.86	1.03	24055
S Pic	423	0.96	0.52	0.62	0.67	3.86	0.88	1.09	24126
T Pic	204	0.86	0.33	0.46	4.29	7.25	0.64	0.78	24468
T Col		0.87	0.35	0.44	1.94	4.93	0.69	0.85	24824
S Ori	413	1.04	0.45	0.48	−0.08	3.08	0.40	0.49	25673
S Col		0.96	0.48	0.57	1.63	4.79	0.55	0.61	27286
U Ori	368	0.96	0.51	0.59	−0.64	2.54	0.84	1.01	28041
V Mon	343	0.84	0.41	0.53	0.97	4.01	0.79	0.90	30326
RV Pup	190	0.89	0.28	0.38	3.53	6.43	0.57	0.68	32115
X Mon	173	0.80	0.25	0.39	2.79	0.00	0.29	0.00	33441
L_2 Pup	137	0.91	0.40	0.57	−2.34	0.73	0.29	0.38	34922
Z Pup	513	1.08	0.59	0.75	1.26	4.53	0.83	1.01	36669
S CMi		0.91	0.42	0.47	0.38	3.46	0.42	0.58	36675
W Pup	120	0.81	0.32	0.48	3.46	6.38	0.49	0.61	37893
SU Pup	333	0.82	0.38	0.51	2.56	5.55	0.84	0.91	38772
R Cnc	362	0.97	0.47	0.53	−0.55	2.60	0.84	1.05	40534
V Cnc	274	1.02	0.36	0.45	3.16	6.23	0.77	0.78	40977
S Hya	255	0.87	0.34	0.46	2.87	5.85	0.55	0.56	43653
T Hya	290	0.89	0.34	0.39	2.36	5.34	0.39	0.49	43835
Y Vel	445	0.98	0.52	0.67	1.07	4.27	0.89	1.05	46502
R Car	307	0.90	0.41	0.47	−1.37	1.68	0.50	0.57	46806
X Hya	307	1.02	0.46	0.52	0.69	3.84	0.45	0.60	46066
R LMi	372	1.11	0.60	0.62	−0.42	2.88	0.71	0.86	47886
R Leo	313	1.03	0.51	0.56	−2.56	0.65	0.50	0.63	48036
S Car	147	0.79	0.25	0.38	1.76	4.55	0.49	0.65	49751
W Vel	381	0.93	0.49	0.47	0.38	3.53	0.97	1.19	50230
S Sex	262	0.94	0.35	0.43	3.48	6.50	0.46	0.57	51791
W Leo	439	0.97	0.49	0.59	1.98	5.15	0.84	0.98	53265
X Cen	340	0.84	0.49	0.59	0.99	4.11	0.67	0.88	57642
W Cen	200	0.86	0.36	0.44	1.88	4.87	0.50	0.61	58107
R Crv	314	0.88	0.38	0.44	1.90	4.92	0.62	0.69	60106
R Vir	148	0.83	0.36	0.46	2.05	5.01	0.62	0.70	61667
R Hya	386	0.98	0.40	0.43	−2.45	0.64	0.43	0.50	65835
S Vir	371	0.94	0.45	0.51	0.41	3.53	0.75	0.85	66100
T Cen	90	0.77	0.23	0.32	2.37	5.12	0.48	0.58	66825
RT Cen	256	0.94	0.32	0.32	2.68	5.66	0.17	0.17	67359
W Hya	361	1.03	0.50	0.54	−3.16	0.06	0.45	0.60	67419
RX Cen	346	0.91	0.48	0.51	2.86	6.00	0.77	0.94	67626
RU Hya	327	0.81	0.45	0.59	1.84	4.91	0.80	0.86	69346
R Cen	531	0.96	0.38	0.41	−0.75	2.31	0.28	0.33	69754
RS Vir	355	0.85	0.53	0.65	1.20	4.37	1.02	1.19	70669
Y Lib	307	0.86	0.45	0.54	3.22	6.31	0.72	0.84	74350
S Lib	201	0.92	0.27	0.30	4.45	7.35	0.54	0.53	75144
RS Lib	218	1.00	0.46	0.49	−0.11	3.04	0.30	0.46	75393
RU Lib	327	0.93	0.38	0.50	2.30	5.35	0.71	0.86	76152

Table 4 – *continued*

Name	P_K (day)	$(J-H)_0$	$(H-K)_0$	$(K-L)_0$	K_0 (mag)	m_{bol}	ΔK	Δm_{bol}	HIP
R Nor	492	1.02	0.34	0.38	1.16	4.29	0.51	0.67	76377
RZ Sco	159	0.83	0.36	0.51	4.12	7.10	0.42	0.51	78746
Z Sco	357	0.98	0.37	0.36	1.44	4.50	0.27	0.31	78872
U Her	407	0.97	0.51	0.63	−0.27	2.96	0.75	0.94	80488
RS Sco	290	0.85	0.46	0.51	0.31	3.39	0.62	0.70	82833
RR Sco	279	0.93	0.41	0.47	−0.29	2.79	0.48	0.57	82912
R Pav	231	0.88	0.39	0.48	2.81	5.84	0.90	1.05	89258
RV Sgr	319	0.93	0.36	0.44	1.63	4.66	0.46	0.54	90493
X Oph	333	0.99	0.41	0.40	−1.02	2.08	0.40	0.45	91389
R Aql	280	0.94	0.45	0.49	−0.72	2.40	0.54	0.66	93820
T Sgr	393	1.13	0.46	0.56	1.33	4.53	0.84	0.86	94706
R Sgr	271	0.87	0.36	0.45	2.02	5.01	0.72	0.77	94738
χ Cyg	399	1.19	0.63	0.72	−1.85	1.48	0.88	0.97	97629
RR Sgr	330	0.84	0.42	0.53	0.66	3.71	0.64	0.77	98077
RR Aql	391	1.00	0.59	0.67	0.46	3.71	0.95	1.17	98220
BQ Pav	109	0.84	0.29		6.52	9.43	0.46	0.67	98447
U Mic	333	0.87	0.50	0.57	1.96	5.10	0.87	1.06	101063
T Aqr	188	0.88	0.36	0.44	3.27	6.27	0.41	0.59	102829
V Cap	276	0.89	0.48	0.59	3.47	6.61	0.78	0.96	104285
T Cap	275	0.91	0.42	0.49	3.25	6.33	0.64	0.83	105498
X Aqr	307	0.87	0.39	0.50	3.00	6.02	0.76	0.88	110146
UU Tuc	326	0.88	0.51	0.65	3.36	6.53	0.82	0.96	110451
RT Aqr	246	0.95	0.34	0.31	2.17	5.17	0.15	0.17	110509
T Gru	143	0.82	0.27	0.46	5.17	8.03	0.50	0.65	110697
S Gru	402	0.95	0.47	0.58	0.73	3.83	1.05	1.19	110736
R Peg	389	0.98	0.54	0.56	0.43	3.66	0.59	0.67	114114
S Peg	321	0.93	0.41	0.44	1.45	4.53	0.48	0.62	115242
R Aqr	393	1.02	0.56	0.80	−1.01	2.23	0.81	0.91	117054

in Fig. 8. There is a general separation between the C stars (lower right) and M stars (upper left), with the S stars falling in between and overlapping both groups. A similar separation is seen in plots of $V-R$ and $R-I$ against period (Barnes 1973, fig. 5). In Fig. 8 the C stars with somewhat redder colours overlapping those of the M stars, R For, RU Vir and V Cyg, have dust shells and their colours show the effects of circumstellar reddening.

Five M stars have long periods and small values of $(Hp-K)_0$ which place them in the region otherwise occupied by C stars: R Cen, R Nor, U CMi, TV Cnc and Z Oph. Of these R Cen and R Nor are known to have double peaked light curves and many of their properties (e.g. relatively early spectral types at maximum of M5e and M3e, respectively) are more characteristic of stars with half the period (Keenan, Garrison & Deutsch 1974). The *Hipparcos* light curves of R CMi (M4e) and Z Oph (K3ep) have bumps on the ascending and descending branches, respectively, making them very similar to double-peaked curves. Colours uncharacteristic of its period were also noted for Z Oph by Barnes (1973). The *Hipparcos* catalogue does not include a light curve for the faint Mira TV Cnc which has been very poorly studied.

For stars with periods below 225 d, there appear to be two approximately parallel sequences of O-rich stars separated by about $\Delta(Hp-K)\sim 2$ mag. This separation is discussed in more detail in Paper II where, for the purpose of establishing the zero-point of the PL relation, the two groups with $\log P < 2.35$, separated by the line $(Hp-K)_0 = 11.7\log P - 19.3$, are treated differently and referred to as the short-period red (SP-red) or short-period blue (SP-blue) stars (see also Section 6.2). The SP-red (*) and SP-blue (#) stars are specifically identified in Table 1.

6 NEAR-INFRARED COLOURS

6.1 Period–colour relations

The various near-infrared period–colour relations are plotted in Fig. 9. The dashed line shown for comparison is the locus for LMC oxygen-rich Miras (Feast et al. 1989, as specified by Glass et al. 1995) and, in the $K-L$ diagram, the dotted line is the locus for Miras in the Sgr I window of the Galactic bulge (Glass et al. 1995).[3] The IR colours of the carbon stars are generally redder than those of the oxygen-rich stars, except in $K-L$ where some C stars are redder and others bluer than the O-rich stars. There is no obvious separation between the SRs and Miras in these diagrams and the S stars have comparable colours to the other O-rich stars. Note in particular the very large scatter in the $K-L$ diagram, much of which is real and not caused by observational scatter, as discussed below. The colours of these local Miras generally lie between those of the bulge and LMC Miras (compare with fig. 4 of Glass et al. 1995). The difference between the colours of the Bulge and LMC Miras is usually attributed to metallicity effects, perhaps a difference in [O/H] (Feast 1996; Feast & Whitelock 2000a), and the colours of the local Miras may indicate that (within the period range sampled by all three groups) their metallicity lies between that of the bulge and the LMC (but see below).

[3] The LMC and bulge data were published on the 1.9-m natural system and must be transformed, as described in a footnote to Section 3.2, for comparison with the data under discussion.

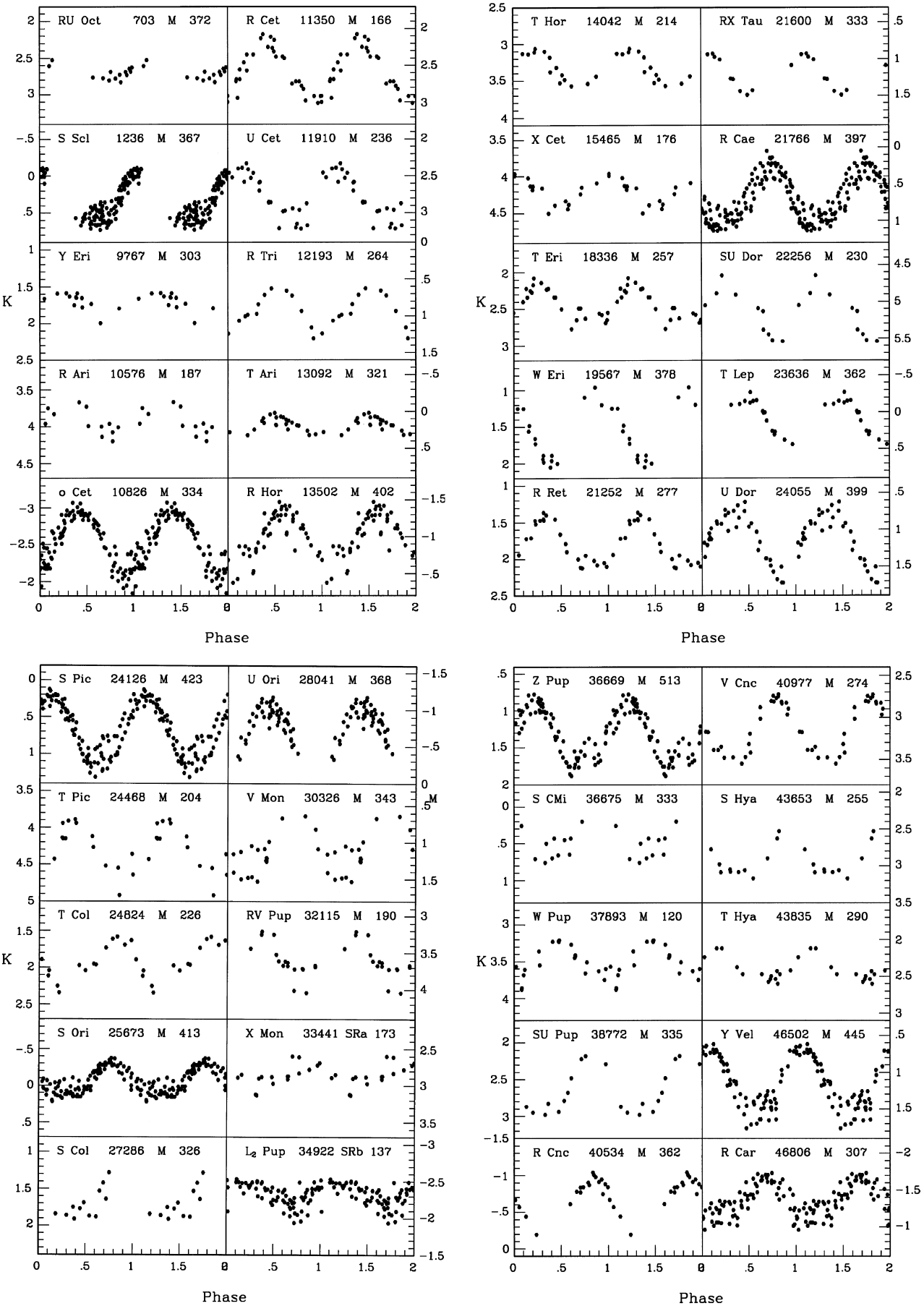

Figure 2. Phased *K* light curves for the O-rich variables with at least 10 SAAO infrared observations. Note that each point is plotted twice to emphasize the variability.

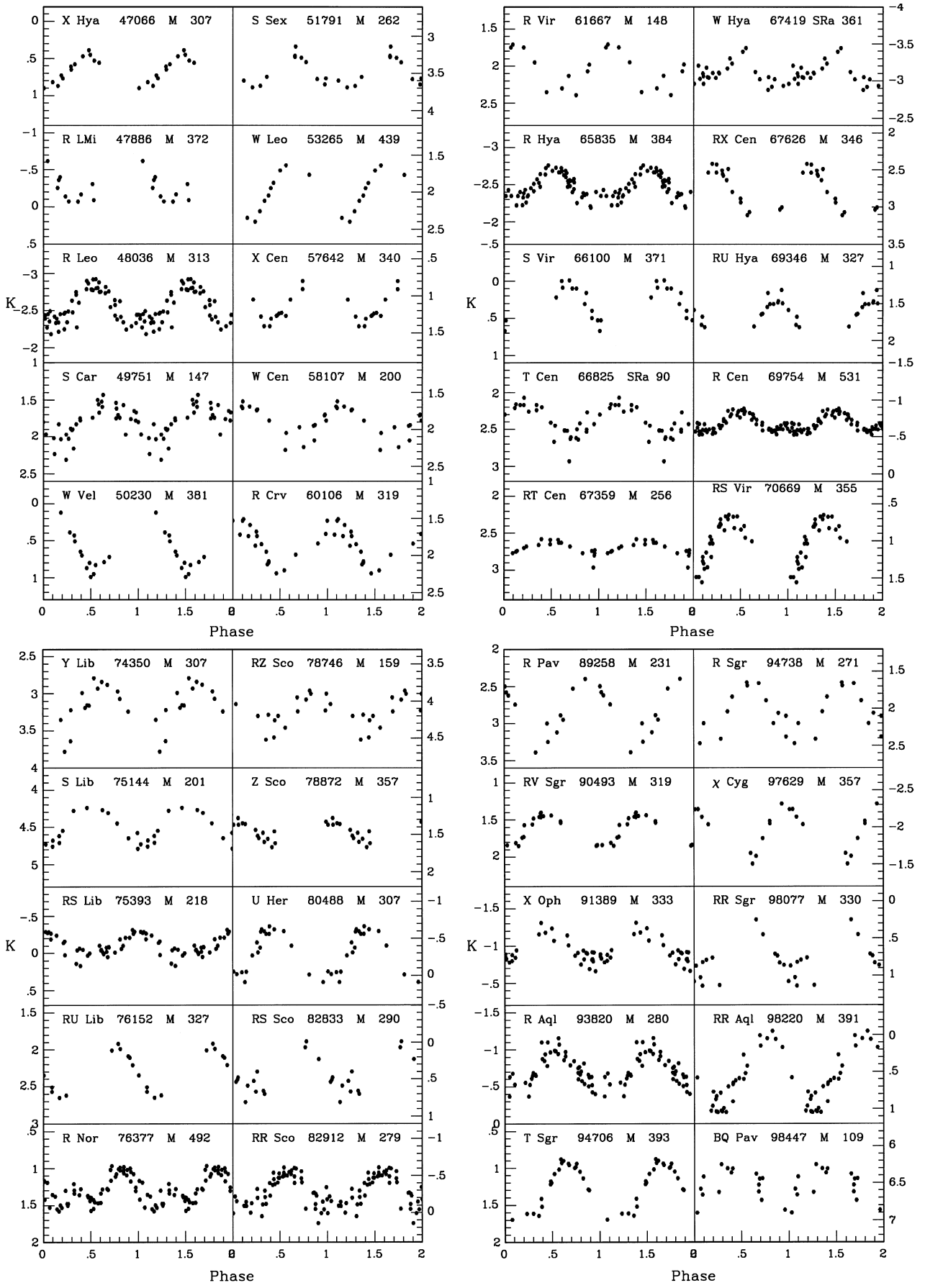

Figure 2 – *continued*

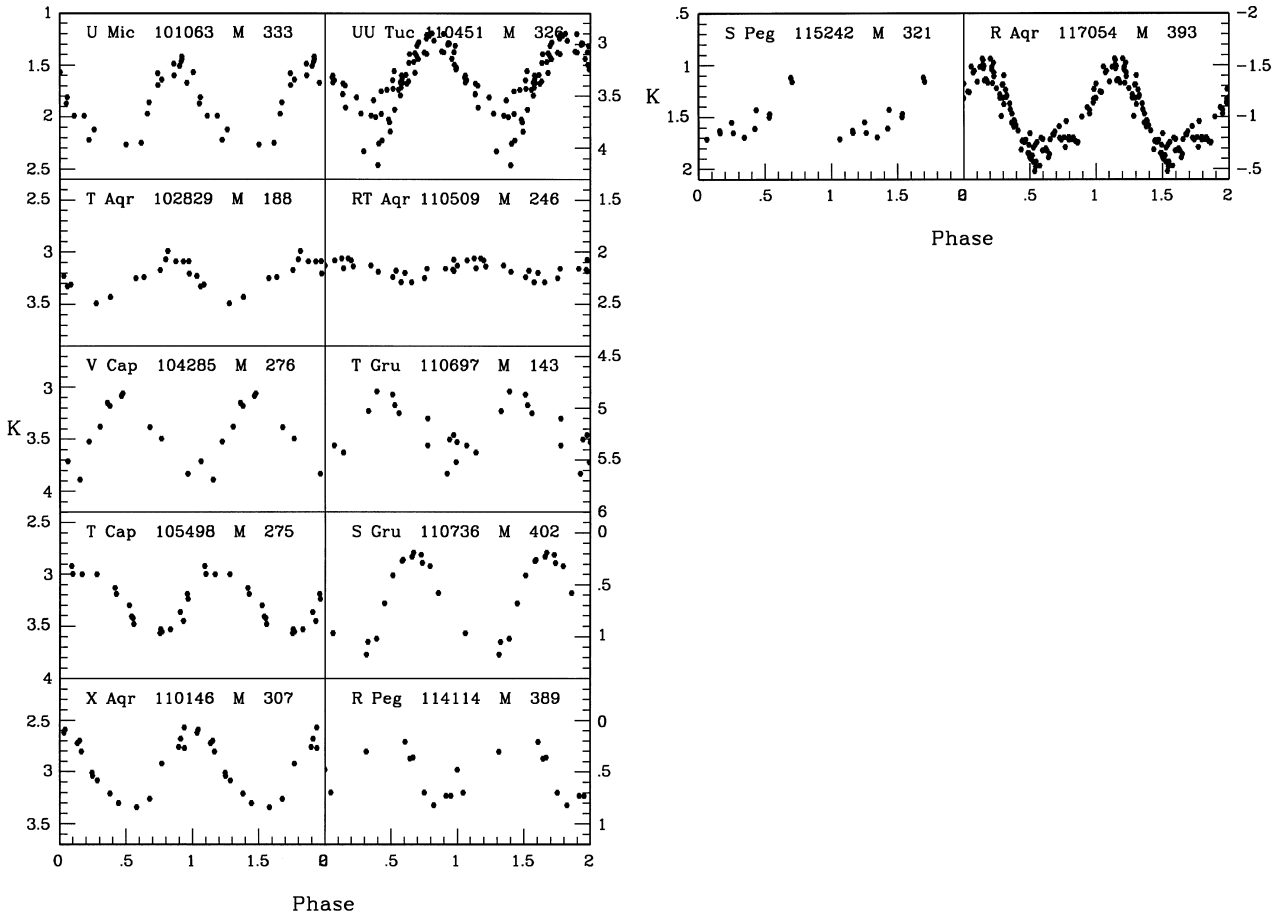

Figure 2 – *continued*

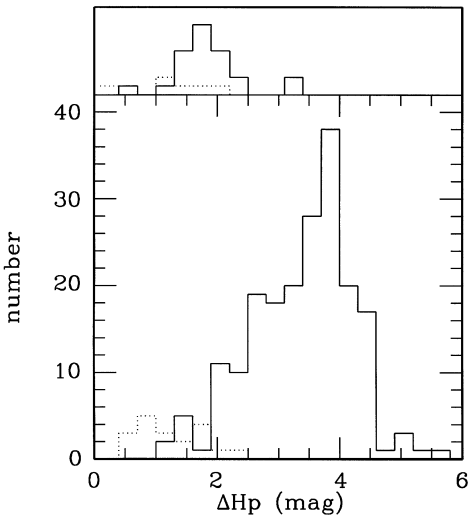

Figure 3. Histogram showing the distribution of *Hipparcos* amplitudes for the oxygen-rich stars (lower panel) and carbon stars (upper panel). The distribution for the Miras is shown as a solid line and that of the other variables as a dotted line.

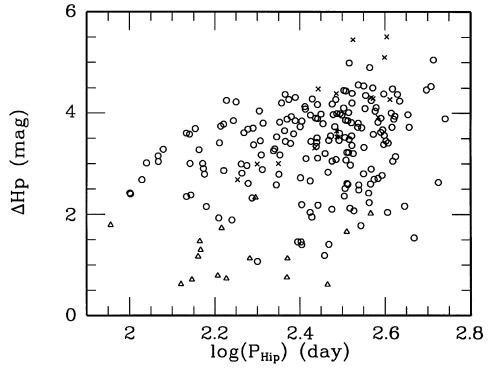

Figure 4. Amplitude of the *Hipparcos* magnitude as a function of period. M-type Miras: open circles; S-type Miras: crosses; M-type SRs: open triangles.

The colours illustrated in Fig. 9 are those corresponding to the mean of the maximum and minimum K magnitude, as were those discussed by Feast et al. (1989), Whitelock et al. (1994) and Glass et al. (1995). It is of interest to examine how the colours at a given period depend on pulsation amplitude, and to do this properly requires as precise an estimate of the colour as possible. We therefore fitted first-order Fourier curves, at the appropriate (IR) period, to the colours for all stars with 10 or more observations (note that using second- or third-order Fourier curves does not significantly change the mean colour). The resulting mean value of each colour is listed in Table 4. It is important to note that all Miras exhibit phase shifts between the curves for different colours, so that the combination of colours shown for any particular star in Table 4 will never actually be measured for that star. Later these

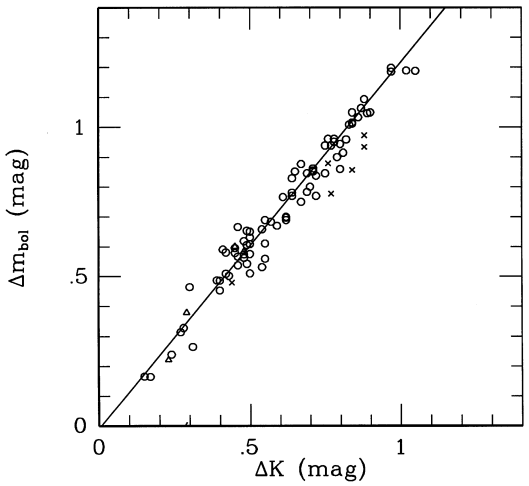

Figure 5. The bolometric amplitude ($\Delta m_{\rm bol}$) as a function of the K amplitude (ΔK); symbols as in Fig. 4.

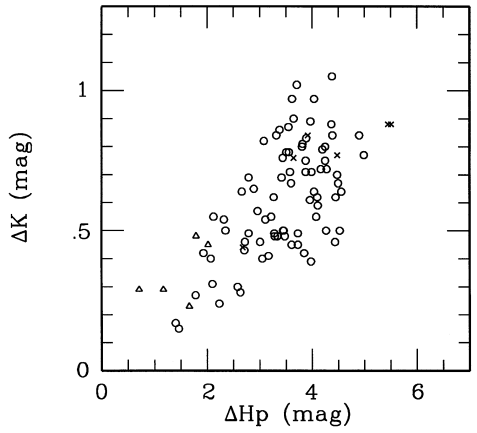

Figure 6. The K amplitude (ΔK) as a function of the *Hipparcos* amplitude (ΔHp); symbols as in Fig. 4.

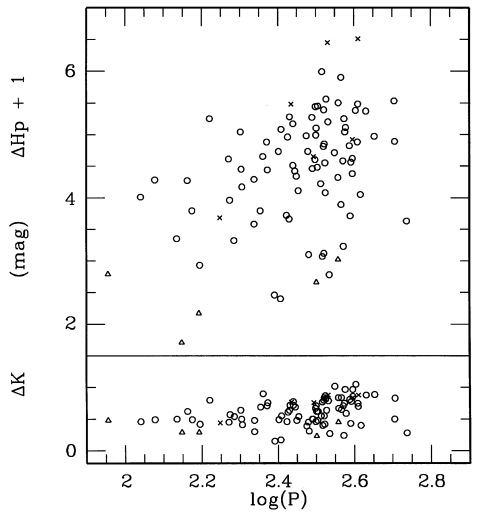

Figure 7. The K and *Hipparcos* amplitude (ΔK, ΔHp) as a function of period, for stars with at least 10 IR observations; symbols as in Fig. 4.

colours are illustrated in a two-colour plot (Figs 13 and 14) and it is obviously not possible to compare any individual measurement of a star with such a plot.

The following period–colour relations for M- (and K-) type Miras are derived by least-squares fitting to the Fourier-mean data:

$$J - H = +0.14(\pm0.09) + 0.32(\pm0.04)\log P; \quad (1)$$

87 stars, $\sigma = 0.054$ mag.

$$H - K = -0.53(\pm0.10) + 0.39(\pm0.04)\log P; \quad (2)$$

87 stars, $\sigma = 0.061$ mag.

$$K - L = -0.21(\pm0.16) + 0.29(\pm0.06)\log P; \quad (3)$$

86 stars, $\sigma = 0.091$ mag.

$$J - K = -0.39(\pm0.15) + 0.71(\pm0.06)\log P; \quad (4)$$

87 stars, $\sigma = 0.090$ mag.

Fig. 10 shows the Fourier-mean colours for the M-type (and K-type) stars as a function of period, for the small-amplitude ($\Delta K < 0.5$ mag) and large-amplitude ($\Delta K > 0.7$ mag) variables only; the K amplitude is, as shown in Fig. 5, directly proportional to the bolometric amplitude for these stars. The dashed lines drawn in these diagrams are the mean relations given by equations (1) to (4). The figure shows distinctly different $J - H$, $H - K$ and $K - L$ colours for the low- and high-amplitude pulsators, at least in the period range 220–560 d. Quantitatively the difference can be evaluated by comparing the zero-points for the period–colour relations derived from the 17 stars with $\Delta K < 0.5$ with those derived for the 26 stars (excluding R Aqr) with $\Delta K > 0.7$, over the period range $2.4 < \log P < 2.7$. The following zero-point differences (ΔZ = large amplitude − small amplitude) are derived: $\Delta Z_{J-H} = -0.052 \pm 0.020$ mag, $\Delta Z_{H-K} = 0.074 \pm 0.019$ mag, $\Delta Z_{K-L} = 0.144 \pm 0.027$ mag, $\Delta Z_{J-K} = 0.021 \pm 0.033$ mag. The difference is significant in all colours except $J - K$. We note that a qualitatively similar difference is seen if the colours derived from Table 3 are used, but in that case the interpretation is complicated by the large scatter.

It is possible to understand the colour differences between the small- and large-amplitude pulsators in terms of differences in the atmospheric extension of the stars, if we assume that those with larger pulsation amplitudes have more extended atmospheres than those with smaller pulsation amplitudes. The effects of photospheric extension on infrared colours were discussed by Bessell et al. (1989). $J - K$ is rather insensitive to extension, but $K - L$ is very strongly influenced by H_2O absorption, increasing rather rapidly as the model becomes more extended. Similarly strong H_2O and CO absorption in extended atmospheres depresses the H flux relative to J and K, producing bluer $J - H$ and redder $H - K$ colours. This is entirely consistent with the observations illustrated in Fig. 10. It is also possible that dust emission makes some contribution to the $K - L$ colours of the reddest stars.

R Aqr, which is the reddest star illustrated in Fig. 10, was omitted from the solutions discussed above because it is a symbiotic Mira in which dust is heated by the compact companion. This modifies its colours, in particular $K - L$, from those of a solitary Mira (Whitelock, Pottasch & Feast 1987).

The fact that, in the $J - K$ period colour relation, there is no significant spread with amplitude indicates that differences in photospheric extension are *not* a factor to be considered in

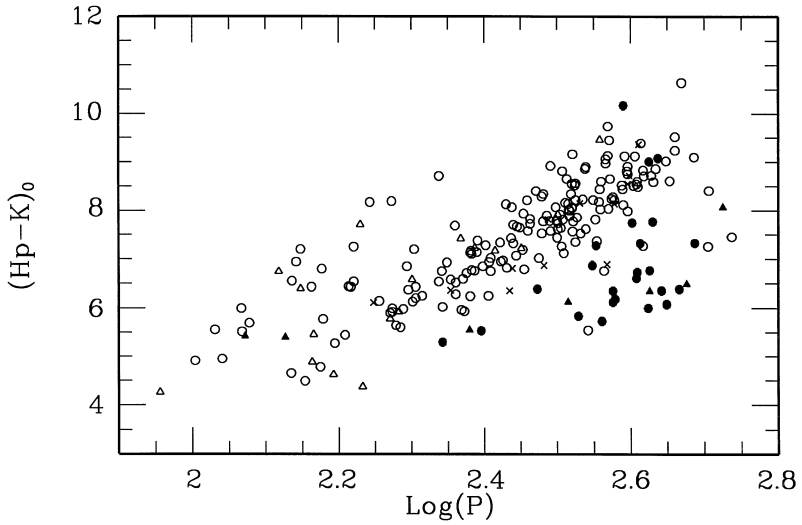

Figure 8. The combined *Hipparcos* near-infrared period–colour relation; open and closed symbols represent O-rich and C-rich stars respectively, crosses represent S stars, circles represent Miras and triangles semiregular variables.

interpreting the period–luminosity–colour relation found for LMC Miras by Feast et al. (1989).

6.2 The SP-red and SP-blue stars

As shown above (Section 5), the *Hipparcos* Miras with periods below 225 d divide into two groups depending on their $Hp - K$ colours. The SP-blue stars have on average an earlier spectral type (M3) than the SP-reds (M4.5) and, as we illustrate in Paper II, different kinematic properties (higher velocity dispersion and asymmetric drift).

In view of the correlation between colour and pulsation amplitude (Section 6.1), it is important to note that the SP-blue and SP-red stars have very similar pulsation amplitudes, before we look at differences in their *JHKL* colours; the seven SP-red stars with Fourier mean colours have $\overline{\Delta K} = 0.49 \pm 0.07$ mag, while the 12 SP-blues have $\overline{\Delta K} = 0.48 \pm 0.03$ mag. So we would not expect colour differences between the SP-blues and SP-reds as a result of atmospheric extension.

The two groups do, however, have slightly different *JHKL* colours at a given period, in the sense that the SP-red group are on average redder than the SP-blue in all colours, as might be anticipated from their $Hp - K$ colours. As there are rather few stars with Fourier-mean colours, this is illustrated in Fig. 11 with the maximum/minimum mean colours derived from the data in Table 3. Note that much of the scatter in this diagram is observational. Nevertheless, in the period range where both SP-red and SP-blue stars are found ($2.1 < \log P < 2.35$) the SP-red stars are on average redder than the SP-blue. This is most clearly illustrated in $J - K$ and presumably indicates a lower effective temperature for the SP-reds. At $\log P \sim 2.25$ the difference between the two groups is $\Delta(J - K) \sim 0.2$ mag which according to Feast's (1996) equation (4) would correspond to $\Delta T_{\rm eff} \sim 700$ K [a similar temperature difference could be derived from the models of Bessell et al. (1989)]. This cannot be interpreted as a simple difference in metallicity between the two groups as we do not see the changes in $J - H$ and $H - K$ that would be anticipated from a metallicity difference (Feast 1996).

Hron (1991) examined the kinematics Miras with pulsation periods in the 150 to 200 d range, dividing them into two groups on the basis of $(V_{\rm max} - K)_0$. He found differences which are consistent with those discussed here and in Paper II. These he interpreted as differences in effective temperature and metallicity in stars from different populations.

6.2.1 *Globular cluster Miras*

The properties, and in the present context particularly the colours, of the Miras found in globular clusters are of particular interest, because these are the only Miras with known metallicity (from the parent cluster). The pulsation period of the star has been shown to be proportional to the metallicity of the cluster (Lloyd Evans & Menzies 1973; Feast 1980; Feast & Whitelock 2000a). Their distances are also known from the clusters, although there remains some uncertainty in the calibration of this distance scale. Within the uncertainties they follow the same period–luminosity relation as do the LMC Miras (Whitelock et al. 1994, fig. 14; Feast & Whitelock 1999).

Menzies & Whitelock (1985) discussed *JHKL* photometry of red variables in globular clusters. The observations listed by them were corrected to the improved standard values as specified by Feast et al. (1989 – Appendix A) and transformed to the SAAO standard system as specified in Section 3.2. Fourier-mean colours were derived and reddening corrections applied using the extinction values specified by Menzies & Whitelock. The results for those Mira variables that have periods and are thought to be cluster members are given in Table 5, together with Fourier-mean magnitudes, K_0, and peak-to-peak amplitudes, ΔK. Note that the phase coverage of the light curves for these cluster variables is not as good as it is for the stars listed in Table 4; given this, and the uncertainties on the various corrections, the *JHK* mean colours are good to only about ± 0.1 mag. There were insufficient L measurements to enable a mean $K - L$ to be derived for the fainter stars, and even for the brighter ones the uncertainty on $K - L$ is high, about ± 0.15 mag.

The colours of the cluster variables, as illustrated in Fig. 11, show no significant departure from the mean relations established for the stars under discussion and specified in equations (1), (2) and (4). In the range of period overlap the 140 to 230 d ($2.15 < \log P < 2.34$) cluster Miras have *JHK* colours very similar to the

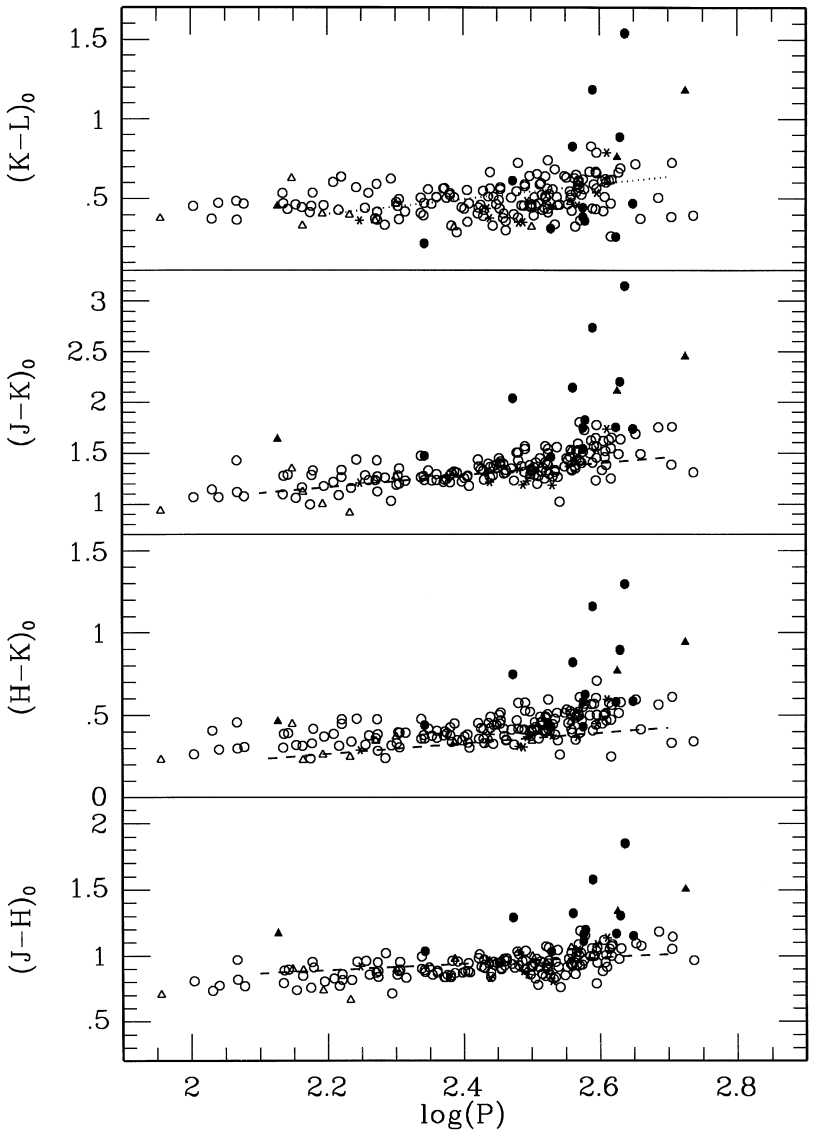

Figure 9. Period–colour relations derived from the data in Table 3; symbols as in Fig. 8. The dashed lines in the lower three plots are the loci for LMC Miras (Feast et al. 1989), while the dotted line on the $K - L$ plot is the relation from Miras in the Sgr I window of the bulge (Glass et al. 1995).

SP-blue group of *Hipparcos* Mira-like variables. This is particularly relevant to the analysis of Paper II, where it is necessary to decide which of the *Hipparcos* Miras should be included in the solution for the zero-point of the PL relation. The information discussed here and in Paper II points towards the SP-blue Miras as being comparable to those found in globular clusters.

6.3 Two-colour diagrams

The near-infrared two-colour diagrams, based on the data in Table 3, are illustrated in Figs 12 and 13. These can be compared with figs 3 and 4 of Whitelock et al. (1994), which show the colours of IRAS-selected Miras in the South Galactic Cap (note that several stars occur in both the *Hipparcos* and the IRAS samples). As one might anticipate, the IRAS-selected sample have on average larger colour indices than do the stars observed by *Hipparcos*. In particular only one star, SS Aqr, in the IRAS group has $(H - K) < 0.45$, whereas about half of the *Hipparcos* sample have $(H - K) < 0.45$.

The carbon- and oxygen-rich stars fall in somewhat different areas of the two diagrams, the differences being most distinct in Fig. 13. The four oxygen-rich Miras which fall in the same region of Fig. 13 as the carbon stars are RU Her, R LMi, R Peg and BG Ser. They are all at high galactic latitudes, $|b| > 40°$, and therefore unlikely to experience significant interstellar extinction. For BG Ser and RU Her there are, respectively, only three and four *JKHL* measures, and although 10 measures were made for the other two stars none of them were close to maximum light. It is thus possible that the colours illustrated for these stars are rather redder than their true mean. There is no reason to think any of them are carbon stars.

The colours of the S-type Miras overlap with those of the other oxygen-rich Miras. The three carbon-rich SRs fall to the upper left of the carbon Miras in Fig. 12 and lower right of them in Fig. 13. This is not obviously significant given the smallness of the sample and that Whitelock (2000) (her fig. 1) found no difference

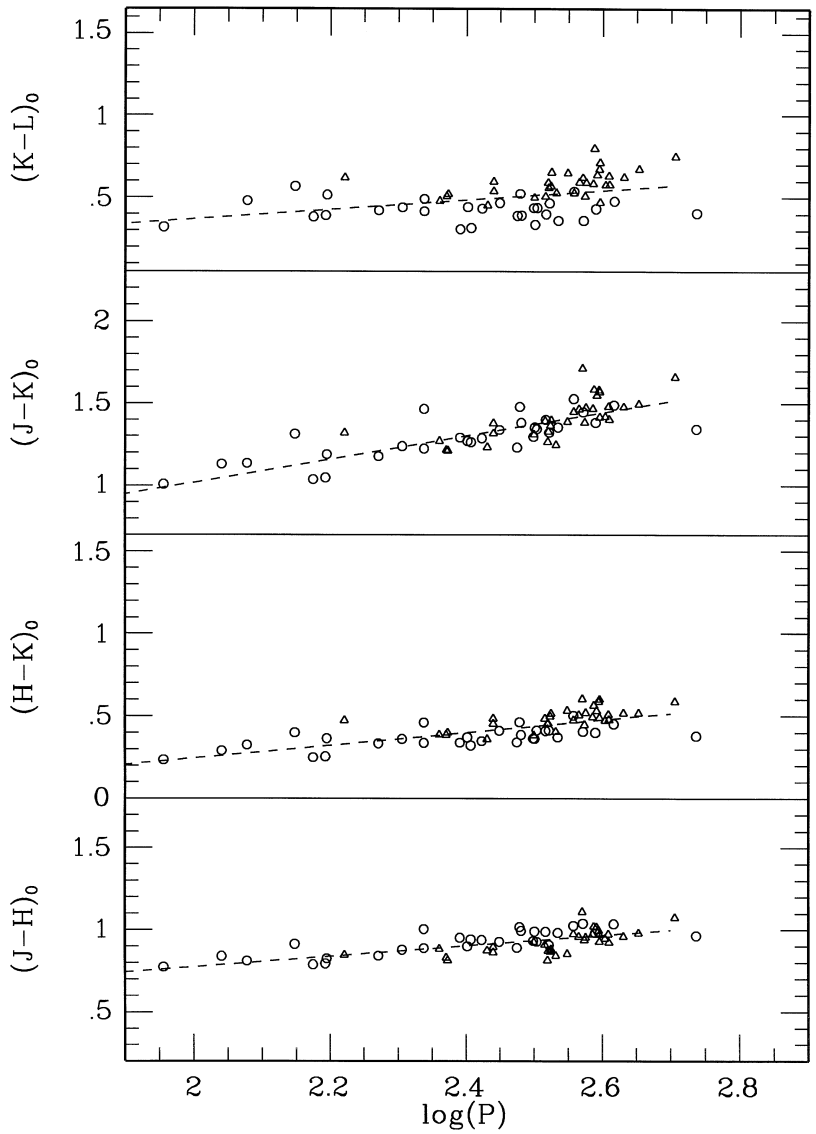

Figure 10. Period–colour relations derived from the Fourier-fit means (Table 4); only M (and K) type, large and small ($\Delta K > 0.7$ mag, triangles, $\Delta K < 0.5$ mag, circles) amplitude variables are shown. The dashed lines are the loci specified in equations (1) to (4).

between the colours of carbon-rich Miras and semiregulars in a larger sample. The oxygen-rich SRs overlap in colour with the Miras although they tend to fall on the lower left side of both diagrams as noted previously by Feast et al. (1982); it should be recalled that the semiregulars under discussion are 'Mira-like' (see Section 2) and not necessarily typical of their class.

The two-colour diagrams for the Fourier-fit mean colours (Table 4) of large- and- small amplitude (see Section 6.1) pulsators are illustrated in Figs 14 and 15. These figures show a very distinct separation in colour between variables with different atmospheric extensions.

Some of the scatter within Figs 12 and 13 is observational; there are points illustrated for stars which have few, sometimes only one, *JHKL* observations at random phases. Nevertheless, a good deal of the scatter must be real and can be attributed to differences in temperature, metallicity and photospheric extension (see e.g. Bessell et al. 1989). For the few star with the highest mass-loss rates ($\dot{M} \sim 10^{-7}\,\mathrm{M}_\odot\,\mathrm{yr}^{-1}$, Section 7), e.g. U Dor and Z Pup, it is possible that circumstellar dust emission also influences the colour (as it does for the symbiotic Mira R Aqr).

6.4 Bolometric corrections

Fig. 16 shows the bolometric correction (BC_K) to the K magnitude as a function of $(J-K)_0$ for the stars with Fourier-mean magnitudes. The curve is a least-squares polynomial which provides a good match ($\sigma = 0.019$ mag) to the data over the range $1.0 < (J-K)_0 < 1.75$:

$$BC_K = 10.86 - 38.10\,K(J-K)_0 + 64.16(J-K)_0^2 - 50.72(J-K)_0^3 + 19.48(J-K)_0^4 - 2.94(J-K)_0^5.$$

The S stars exhibit on average a slightly smaller ($\Delta K \sim 0.03$ mag) correction than do the other O-rich stars, but there are too few S stars to be sure that this is significant.

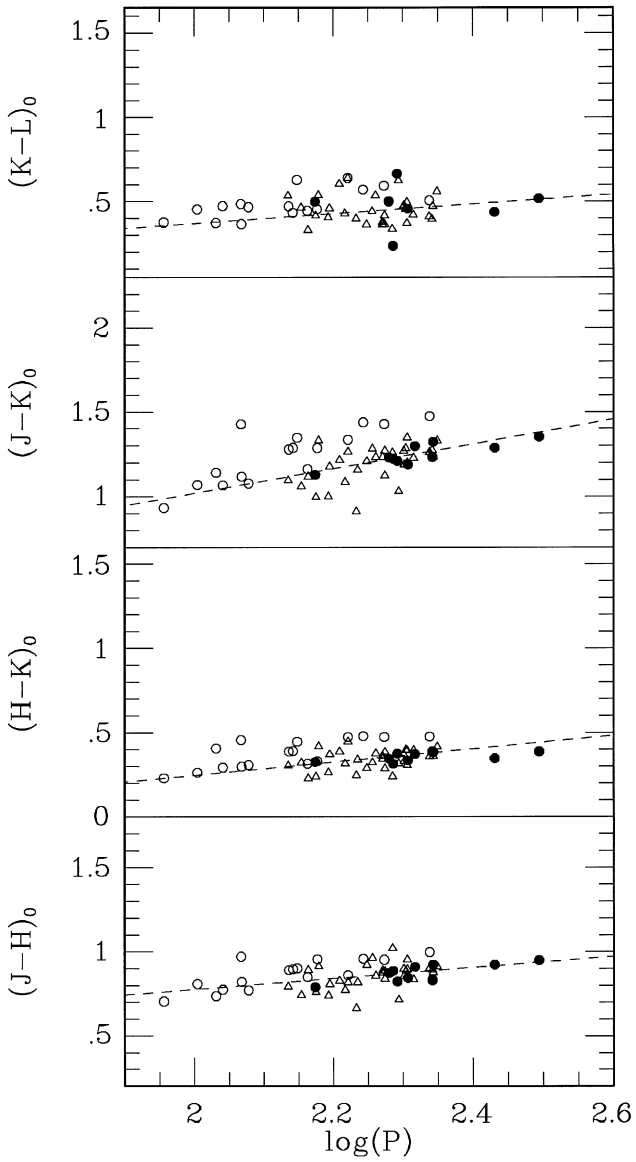

Figure 11. Period–colour relations for the SP-red (open circles), SP-blue (open triangles) and globular cluster variables (closed circles). The dashed lines are the mean relations described by equations (1) to (4). The SP-blue and SP-red colours are derived from the maximum/minimum means of Table 3, while the cluster data are Fourier means from Table 5.

Table 5. Fourier means for globular cluster Miras.

Name	$(J-H)_0$	$(H-K)_0$	$(K-L)_0$ (mag)	K_0	ΔK	P (day)
N104V2	0.84	0.34	0.46	6.28	0.52	202
N5139V42	0.79	0.33	0.50	7.38	0.92	149
N5927V3	0.95	0.39	0.52	7.14	0.70	311
N6356V3	0.83	0.39	–	8.95	0.49	219
N6356V4	0.91	0.37	–	8.92	0.65	207
N6356V5	0.92	0.39	–	8.95	0.79	220
N6553V4	0.92	0.35	0.44	6.11	0.56	269
N6637V4	0.82	0.38	–	7.91	0.48	195
N6712V7	0.87	0.34	0.50	7.34	0.70	190
N6838V1	0.89	0.31	0.24	6.22	0.18	193

7 *IRAS* COLOURS AND MASS-LOSS

Most of the stars under discussion have fluxes listed in the *IRAS* Faint Source Catalogue (Moshir 1989) or the Point Source Catalogue. The 12-μm magnitude, [12], was calculated as described in the explanatory supplement to the Point Source Catalogue (IRAS Science Team 1988) after colour correcting the data. The colour correction for stars with no 25-μm flux was calculated assuming $F_{12}/F_{25} = 2.58$, which was the mean value for the 203 stars that had $F_{25} > 2$ Jy. A $K_0 - [12]$ colour can then be evaluated for 231 stars. This is shown in Fig. 17(a) as a function of pulsation period.

Whitelock et al. (1994) showed that $K_0 - [12]$ was a function of mass-loss rate and Le Bertre & Winters (1998) extended this work to lower mass-loss rates. Blackbodies with temperatures between 2000 and 3000 K would have $1.6 > K - [12] > 0.9$ and

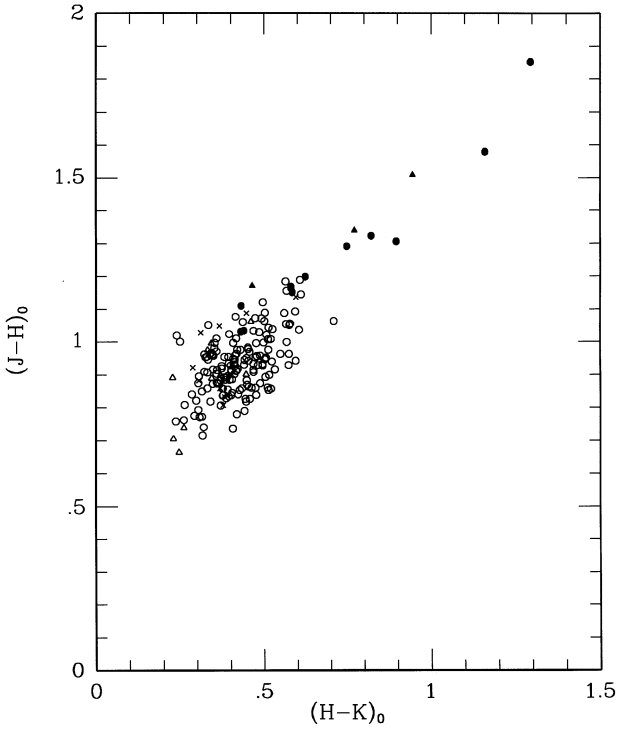

Figure 12. Near-infrared two-colour diagram based on the data from Table 3. Symbols as in Fig. 8.

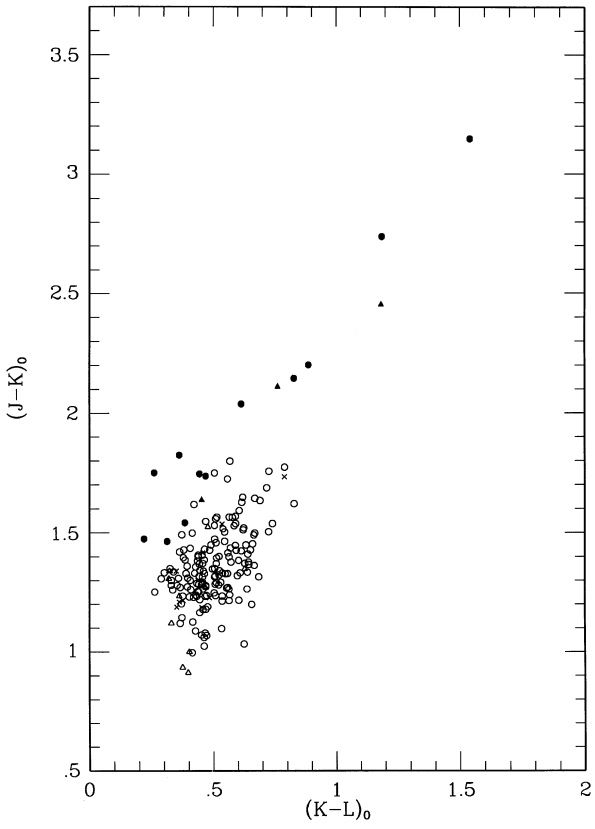

Figure 13. Near-infrared two-colour diagram based on the data from Table 3. Symbols as in Fig. 8.

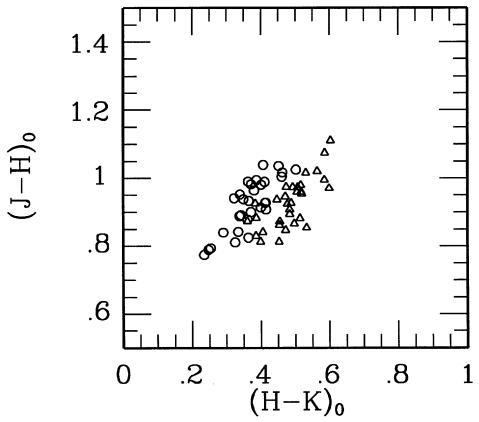

Figure 14. Near-infrared two-colour diagram based on the data from Table 4. Only the large and small amplitude pulsators are illustrated. Symbols as in Fig. 10.

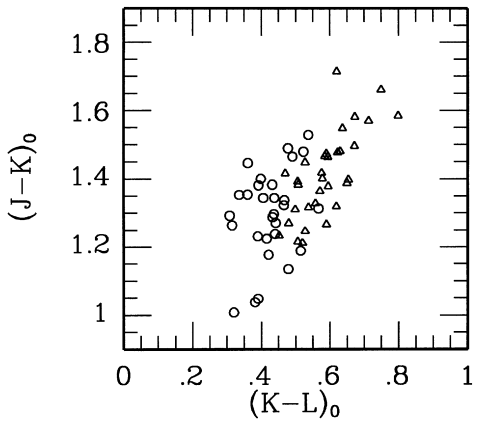

Figure 15. Near-infrared two-colour diagram based on the data from Table 4. Only the large and small amplitude pulsators are illustrated. Symbols as in Fig. 10.

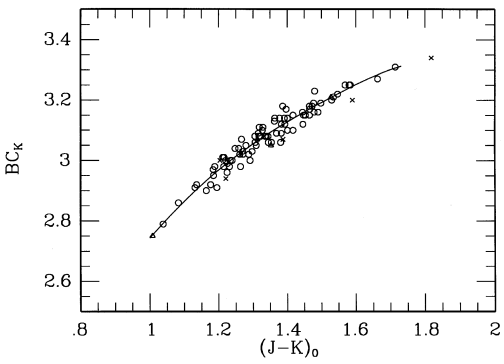

Figure 16. The *K* bolometric correction as a function of colour for the stars with data in Table 4.

the colours of many of the stars fall within this range. Some scatter will be introduced in this diagram because of the limited phase coverage of the measurements, particularly those from IRAS, and the non-simultaneous nature of the IRAS and *K* measurements. It is not possible to calculate the mass-loss rates for these stars in the same way as did Whitelock et al. (whose sources were selected as

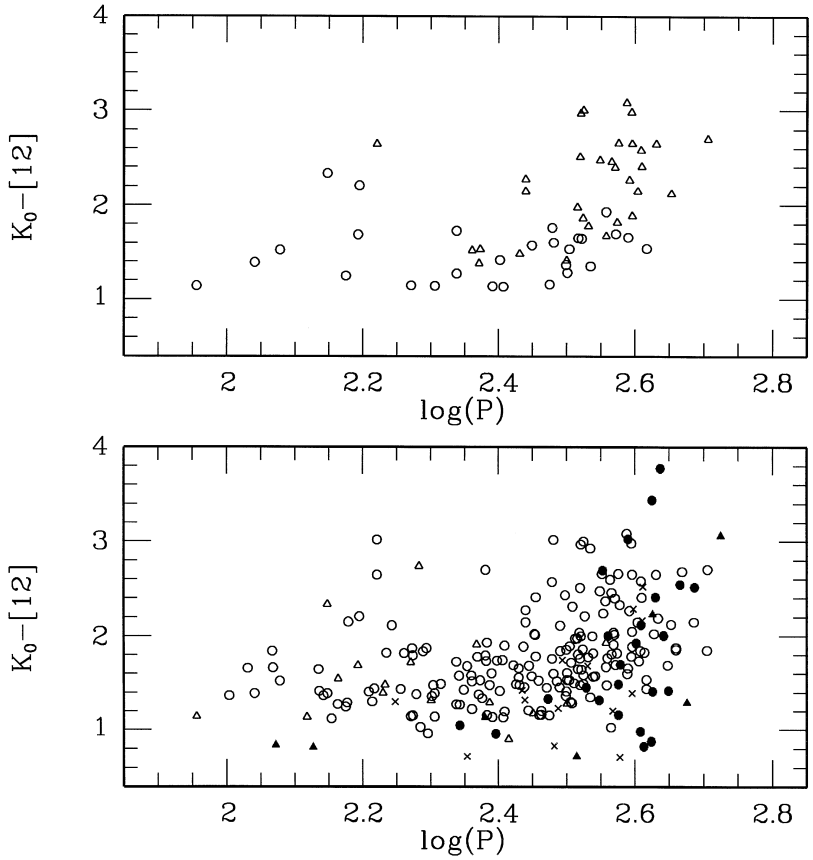

Figure 17. (a) $K_0 - [12]$ (a function of mass-loss rate) against log period for all stars with the relevant photometry. Symbols – M-type Miras: open circles, C-type Miras: closed circles, S-type Miras: crosses, other O-rich variables: open triangles, other C-rich variables: closed triangles. (b) $K_0 - [12]$ as a function of period for the large amplitude (triangles: $\Delta K > 0.7$ mag) and small amplitude (circles: $\Delta K < 0.5$ mag) variables.

having 25-μm flux at least half the 12-μm flux) because we cannot assume that the 25-μm flux, or even the 60-μm flux, originates largely from the circumstellar dust in these thin-shelled sources. By comparison with fig. 21 of Whitelock et al. and Le Bertre & Winters (who do not colour-correct the IRAS data) we can deduce that most of the stars under discussion have $\dot{M} < 10^{-7}\,\mathrm{M}_\odot\,\mathrm{yr}^{-1}$ and that many of them have negligible mass-loss rates.

The majority of stars with higher mass-loss rates occur at longer periods, $P > 300$ d, although there are low mass-loss stars over the whole period range. There are several stars with periods around 130 to 190 d ($2.13 \lesssim \log P \lesssim 2.28$) which have surprisingly high $K - [12]$, including two semiregular variables, L_2 Pup and V CVn.

The plot of $K - [12]$ against $\log P$, illustrating only those M- (or K-)type stars with large or small K amplitudes, Fig. 17(b), indicates that, in general, the stars with larger amplitudes have larger $K - [12]$ and vice versa, although the short-period low-amplitude SRs, L_2 Pup and RZ Sco, stand out as exceptions. A comparison with a similar diagram separating the stars on the basis of their *Hipparcos* amplitude (not shown) indicates that ΔK is a better indicator of high $K - [12]$ than is the *Hipparcos* amplitude, ΔHp.

Note that the $K - [12]$ versus mass-loss calibration may not work for the symbiotic stars, such as R Aqr and possibly even o Cet (where the dust shell is heated by the white dwarf companion with which the Mira is weakly interacting).

The S stars typically show rather lower values of $K_0 - [12]$ than do the M stars, while C stars cover the full range exhibited here. M-type non-Mira variables typically have small values of $K_0 - [12]$, although V CVn and L_2 Pup are notable exceptions to this.

Fig. 18 shows that $K - L$ varies rather closely with $K - [12]$, and that the larger amplitude pulsators have redder colours. Note that the red $K - L$ colours cannot be a consequence of circumstellar reddening because the other near-IR colours would be similarly affected, but the stars with large pulsation amplitudes have relatively blue $J - H$ colours. Detailed modelling is required to see if the extreme $K - L$ colours are influenced by dust emission in L or if they can be understood entirely as the result of atmospheric extension (Section 6.1). Dust formation and mass-loss will occur more easily in a more extended atmosphere and result in the larger $K - [12]$ colours seen in the stars with extreme $K - L$.

Whitelock et al. (1987) showed that the mass-loss rate from Miras depended on both the luminosity and pulsation amplitude of the star. This was interpreted as a direct demonstration of the importance of pulsation as a mechanism for driving mass loss. The results under discussion, which associate pulsation amplitude, *atmospheric extension* and mass loss, suggest a slightly modified interpretation. It seems plausible to suggest that large-amplitude pulsation produces a star with with extreme atmospheric extension. This in turn provides a low-temperature, high-density environment in which dust can condense. Mass loss will then be

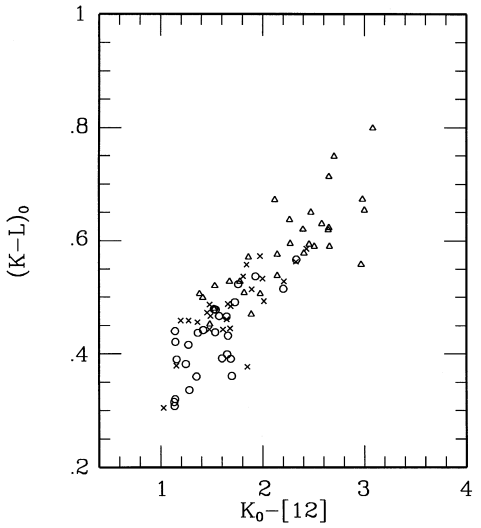

Figure 18. $(K-L)_0$ vs $K_0-[12]$ for the M-type variables; triangles represent large amplitude ($\Delta K > 0.7$ mag) and circles small amplitude ($\Delta K < 0.5$ mag) variables, while intermediate amplitudes are represented by crosses.

driven by radiation pressure on the dust, which is dynamically coupled to the gas.

8 S STARS

The number of S stars in the survey is rather too small to draw useful statistical conclusions from. The are 10 stars with SAAO photometry: X Cet, R Gem, V Gem, V Cnc, S Her, T Sgr, χ Cyg, X Aqr, SU Pup, SX Peg, and an additional four with K measurements from elsewhere: R And, W And, R Lyn, S UMa. *Hipparcos* also observed CN Cyg, but no IR photometry is available for this star.

A few general trends are notable. The amplitudes, ΔHp and ΔK, are typically larger at a given period than are those of the other O-rich Miras. χ Cyg and SU Pup have the largest Hp amplitudes of any of the Miras; indeed χ Cyg is also well known for its particularly large visual light range. The K amplitudes are not quite so extreme and the bolometric amplitudes are more or less the same as those of the other O-rich stars. Thus the extreme Hp amplitudes in the S stars must be a consequence of the changing strengths of molecular bands around the pulsation cycle, rather than of extreme temperature changes.

Some, although not all, of the S stars stand out in Fig. 17 as having particularly low values of $K-[12]$ and presumably low dust mass-loss rates. Although not shown in Fig. 18, T Sgr ($K-L=0.56$, $K-[12]=1.39$) and χ Cyg ($K-L=0.72$, $K-[12]=2.16$) fall outside the area occupied by the colours of the other stars; they have low $K-[12]$ for their $K-L$.

One might anticipate that the S stars, which have C/O ~ 1 (owing to dredge-up of C-rich material), would have lower dust-to-gas ratios than stars with higher or lower C/O ratios (because almost all the carbon and oxygen will be tied up in the CO molecule and therefore not available for forming either C- or O-rich dust). If this were the case then $K-[12]$ would provide only a lower limit to the total mass-loss rate. However, Groenewegen & de Jong (1998) find, with certain assumptions, dust-to-gas ratios for a sample of S-type Miras that are similar to C- or O-rich Miras.

It is worth a particular note on χ Cyg. Its near-IR colours are all unusually red, in particular the Fourier mean $J-K$, 1.84, is 0.38 mag redder than the value given by equation (4). There are only 11 observations of χ Cyg, and the mean $J-K$ may have been overestimated, but the error is unlikely to be over 0.05 mag. Being rather far north, the star is quite difficult to observe from SAAO and its magnitudes may therefore be more uncertain than those of other stars, but a comparison with observations by Yudin (private communication) from the Crimea Observatory suggests that errors in excess of 0.05 mag in the colour are unlikely. Neither is there any reason to believe its interstellar reddening could be greater than the assumed value. The low value of $K-[12]$ is not consistent with a thick circumstellar shell unless it were very asymmetric and concentrated in the line of sight. Groenewegen & de Jong (1998) find a higher mass-loss rate ($\sim 2\times10^{-7}\,M_\odot\,yr^{-1}$ at 180 pc) for χ Cyg than $K-[12]$ would suggest [$\sim 4\times10^{-8}\,M_\odot\,yr^{-1}$; Le Bertre & Winters (1998)], but with a high gas-to-dust ratio ($\sim 10^3$). This does not provide any particular support for asymmetric mass loss in χ Cyg.

9 LONG-TERM TRENDS

The light curves of oxygen-rich stars with at least 60 *JHKL* observations were examined for long-term trends and the results are discussed briefly below. The light curves of four of the carbon Miras included in this analysis (R For, R Lep, RV Cen and V Cru) were discussed by Whitelock et al. (1997), while that of the symbiotic Mira, R Aqr, was discussed by Whitelock (1999).

The long-term trends in the visual light curves of various Miras were discussed by Mattei (1997) and elsewhere (e.g. Bedding et al. 2000). Visual magnitudes for many bright Miras are available over very long time periods and with much better phase coverage than the infrared data presented here. Visual data are unquestionably important in looking for evolutionary and other long term changes in the light curves. However, the *JHKL* observations are of higher precision than the visual magnitudes and provide us with a much better indication of changes in the bolometric luminosity (the light output of these stars generally peaks between 1 and 2 μm). In particular, the relative effect of changes in temperature, molecular band strengths and radius are quite different in the two spectral regions. The observations presented here cover a longer time period than has been previously available and will provide an important database for comparison with unusual variables.

The data are discussed in terms of Fourier components. In general the infrared variations of Miras are more nearly sinusoidal than are their visual variations. Nevertheless, the departure from simple sinusoids is illustrated below by the presence of significant harmonics in the light curves. A number of stars also show some evidence for subharmonics in the light curves, in particular at twice the main pulsation period. In almost all cases the residuals from the fits are higher than one would expect from observational uncertainty (see Section 3.2), indicating that there are erratic changes in the bolometric luminosity as there are in the visual light.

The existence or otherwise of long term trends in light curves of oxygen-rich Miras is of considerable interest in comparing them with carbon-rich and symbiotic Miras. Some carbon Miras go through prolonged faint phases, possibly because of the ejection of discreet puffs of dust (Whitelock et al. 1997), behaviour which is reminiscent of RCB stars, while some oxygen-rich symbiotic Miras show what have been described as 'obscuration events',

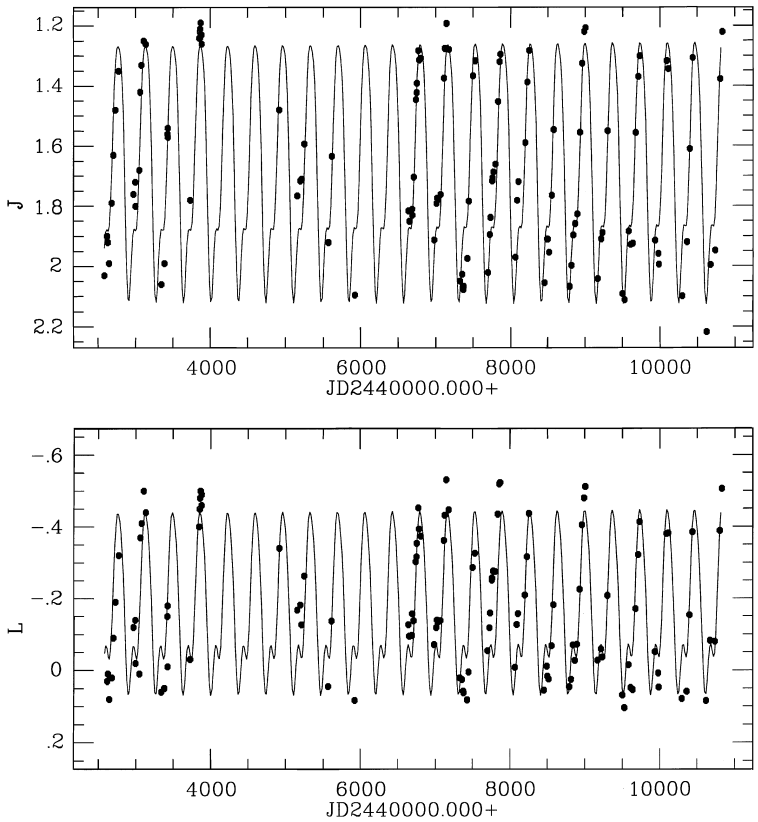

Figure 19. The light curve for S Scl at (a) *J* and (b) *L*.

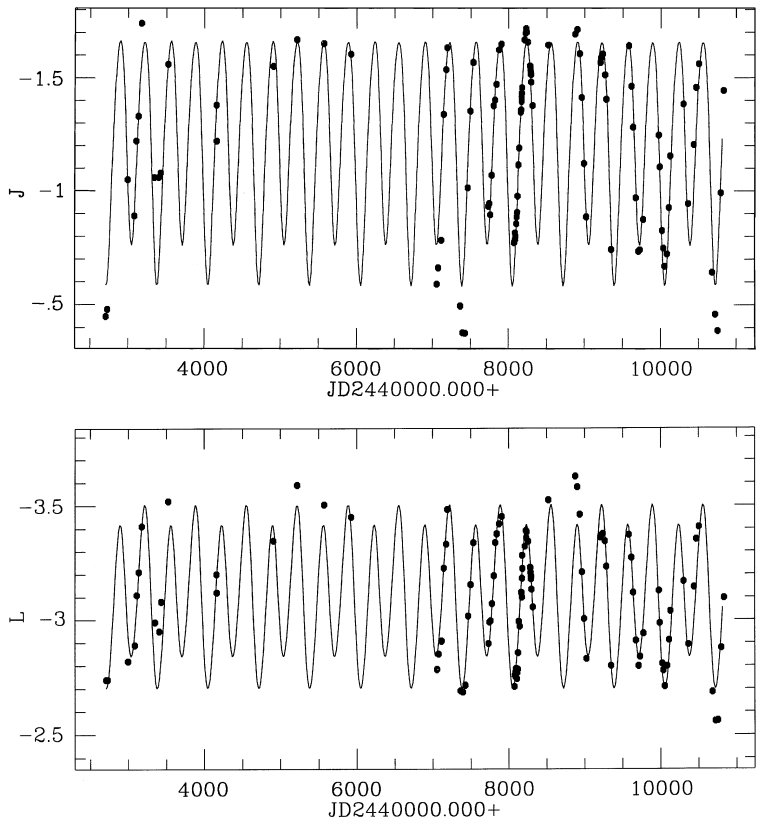

Figure 20. The light curve for *o* Cet at (a) *J* and (b) *L*.

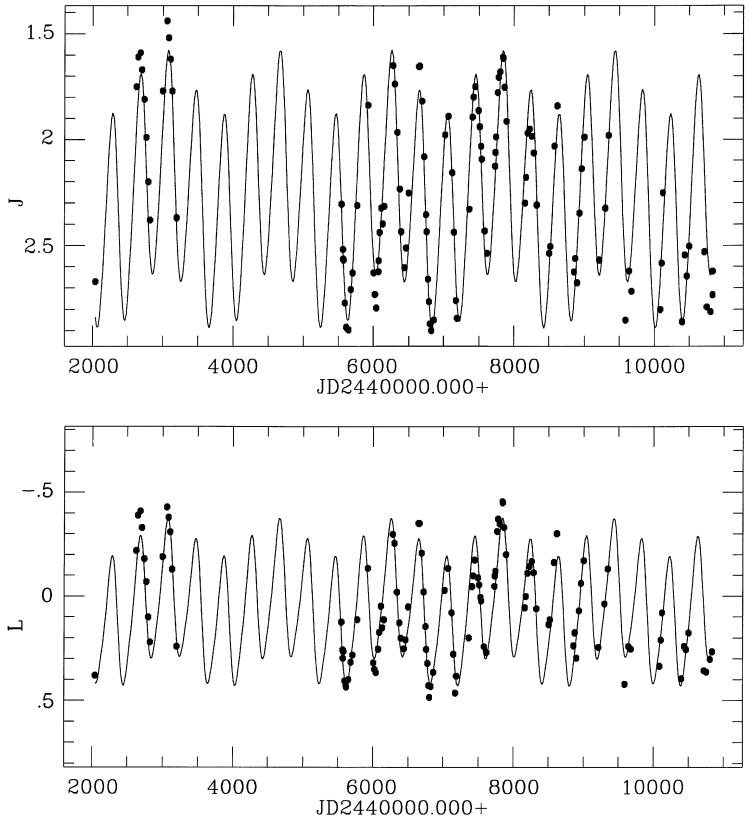

Figure 21. The light curve for R Cae at (a) *J* and (b) *L*.

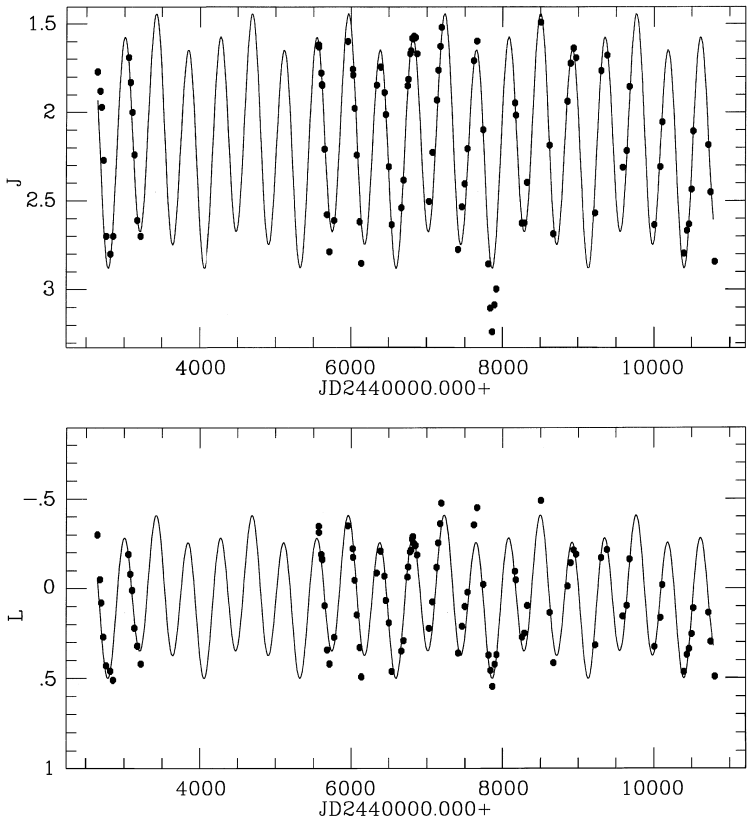

Figure 22. The light curve for S Pic at (a) *J* and (b) *L*.

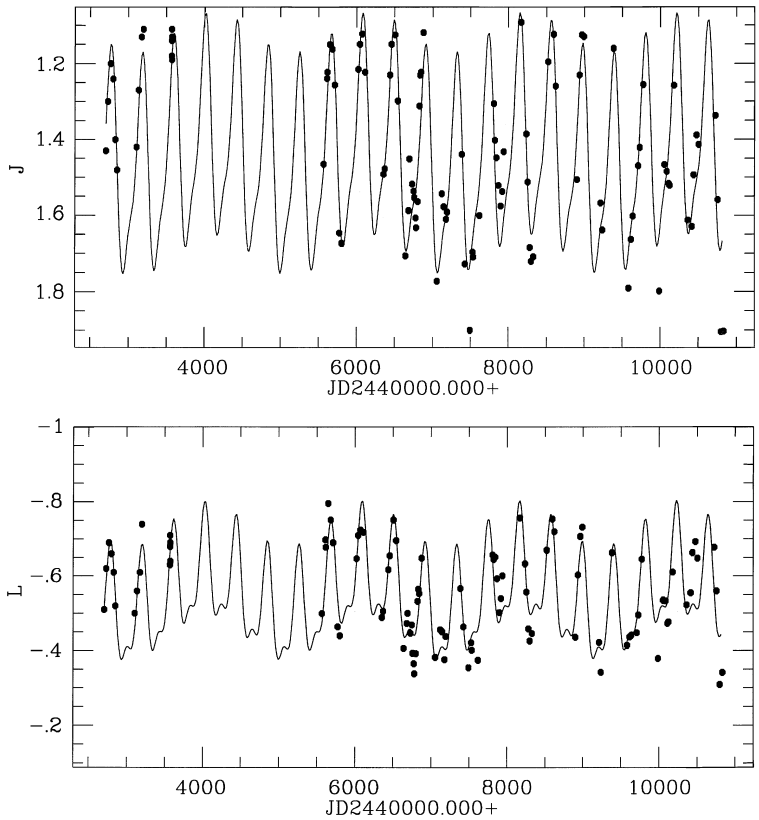

Figure 23. The light curve for S Ori at (a) *J* and (b) *L*.

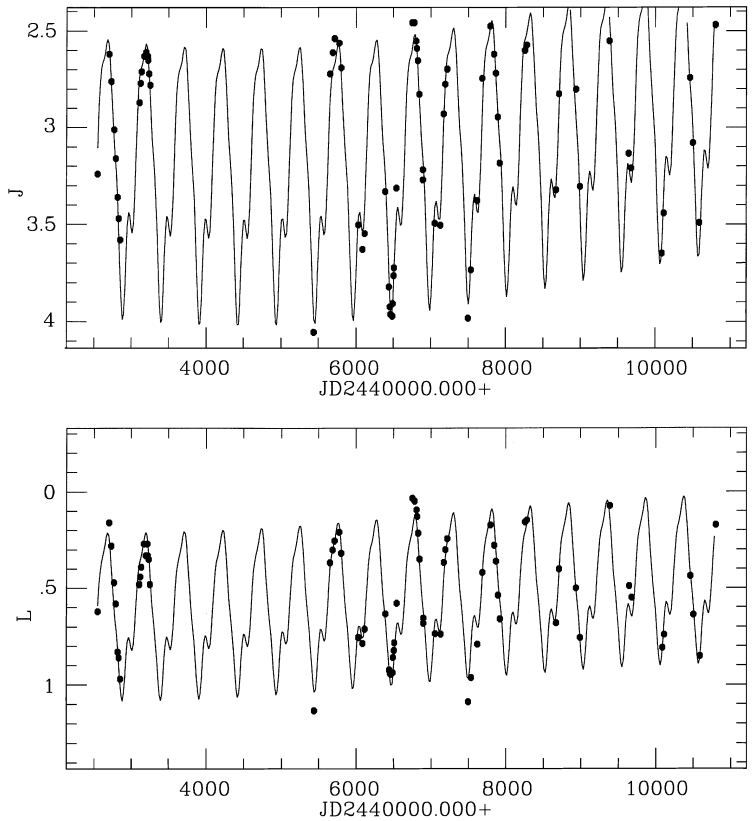

Figure 24. The light curve for Z Pup at (a) *J* and (b) *L*.

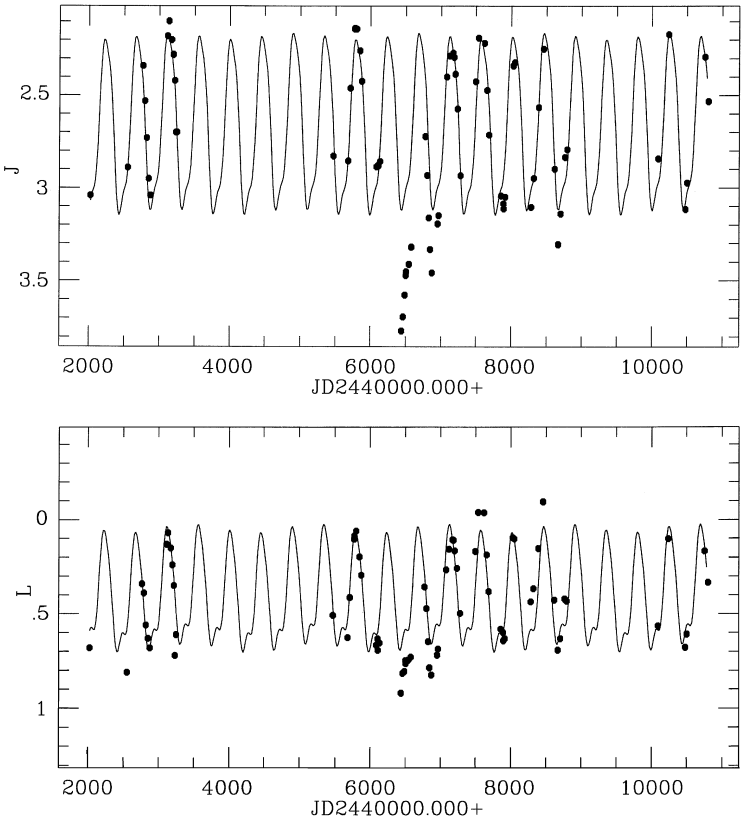

Figure 25. The light curve for Y Vel at (a) *J* and (b) *L*.

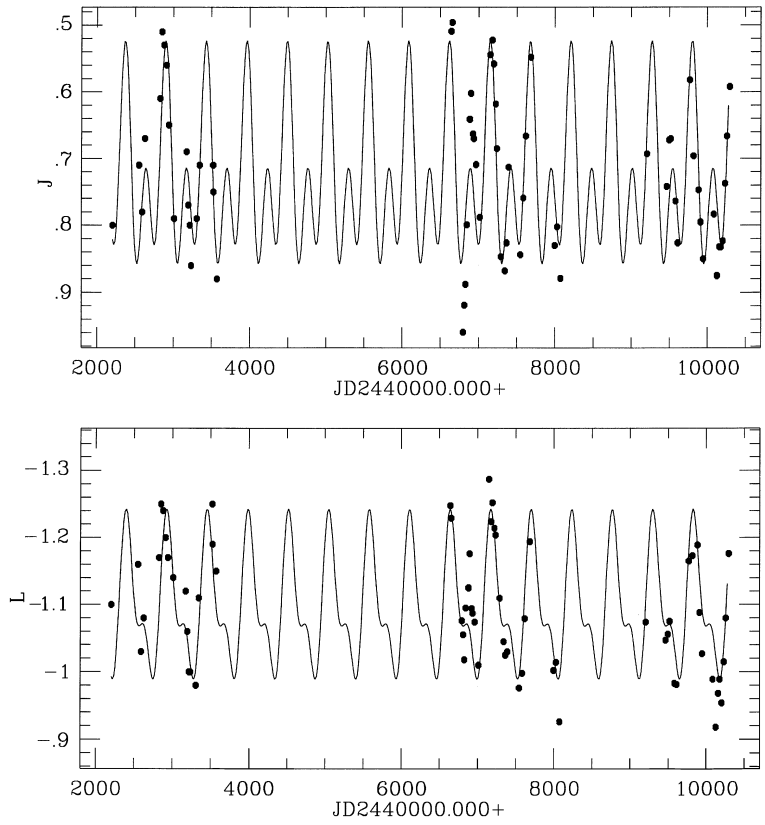

Figure 26. The light curve for R Cen at (a) *J* and (b) *L*.

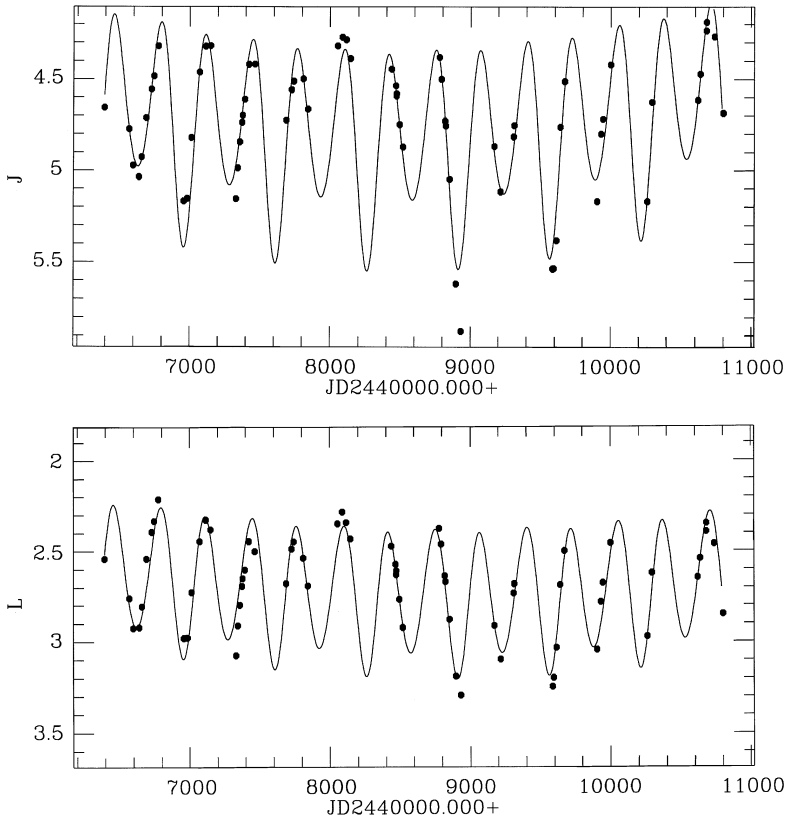

Figure 27. The light curve for UU Tuc at (a) *J* and (b) *L*.

which may be related to orbital effects in the binary systems (Whitelock 1987).

There is little evidence in the data presented here for major obscuration events, except perhaps in Y Vel.

S Scl. the 121 observations cover 22 yr. The period is sufficiently close to a year that the falling branch has never been observed. The *J* and *L* curves are illustrated (Fig. 19) with best-fitting sine curves of period 367 d and the first two harmonics *P*/2 and *P*/3 (the second is more important than the first); the residuals from these curves are 0.09 mag in both colours. No other systematic trend is evident.

***o* Cet.** The curves shown in Fig. 20 are 334-d sines with first harmonics and subharmonics, i.e. *P*, *P*/2 and 2*P*. The residuals are significant, 0.12 mag at *J* and 0.09 mag at *L*, but there are no systematic trends or significant other periods. The inclusion of the subharmonic improved the residuals by about 0.02 mag, and is responsible for the alternating deep and shallow minima. Barthés & Mattei (1997) analyses the long term variations in the AAVSO light curve, a very extensive data set, of this star.

R Hor. (not illustrated). These data were obtained in two batches which yield slightly different periods, 392 and 402 d for the first 22 and last 29 points respectively.

R Cae. The best-fitting pulsation period is $P = 397$ d; the fit shown in Fig. 21 is a combination of *P*, *P*/2, 4*P*. It has a residual of 0.12 and 0.08 mag at *J* and *L* respectively. The residual at *J* is improved by 0.04 mag when 4*P* is included in the fit. This is marginally significant and more data are required to establish the reality of this period. A very slight improvement ($\sim$0.01 mag) can be achieved with an additional long term trend.

S Pic. The pulsation period is $P = 423$ d, and the fit illustrated in Fig. 22 is a combination of this and 3*P*, although a slightly better fit ($\lesssim$0.01 mag) is achieved if a second period of 1371 d is used rather than 3*P*. The residuals are 0.13 and 0.09 mag at *J* and *L* respectively. There was a particularly deep minimum around JD 244 7900 during which the colours were redder and which is the major cause of the high residual in the *J* fit.

S Ori. The curve illustrated in Fig. 23 comprises $P = 413$ plus *P*/2 and 5*P*. The residuals from this are 0.08 mag at *J* and 0.06 mag at *L*. The improvement achieved in the residuals by adding 5*P* is quite small ($\lesssim$0.01 mag at *J* and $\gtrsim$0.01 at *L*), and not obviously significant. The pulsation amplitude of S Ori is particularly low ($\Delta J = 0.55$ mag), and the behaviour of the light curve suggests the interaction of a second period with the main pulsation. Many more observations, and particularly maxima and minima around the same cycle, are required to investigate this. Percy & Colivas (1999) suggest, from an analysis of the AAVSO data, that the period of S Ori is changing, as do Bedding et al. (2000).

Z Pup. The curve in Fig. 24 shows the fit of $P = 512$ plus *P*/2, *P*/3 and *P*/4 together with a long term trend. The residuals are 0.09 mag at *J* and 0.07 mag at *L*. A reasonable fit is also provided using a period of 476 d in place of the long term trend, which produces a very different appearance and a residual of 0.09 mag at *J*.

Y Vel. The curves illustrated in Fig. 25 are $P = 443$ plus *P*/2 and *P*/3. These provide a reasonable fit except around JD 244 6500. Between JD 244 6136 and 244 6440 the *J* light faded by about 0.65 mag and gradually returned to normal over the next 800 d. *L* faded by about 0.2 mag and recovered over the same period of time. This may be an example of a oxygen-rich star

undergoing a dust obscuration event of the type that seems relatively common in carbon stars (Whitelock et al. 1997).

R Cen: The fits shown in Fig. 26 are for $P = 531$ d and $P/2$; the first harmonic is very prominent (as it is in the visual light curve). The residuals from these curves are 0.06 and 0.05 mag at J and L respectively. A slightly better fit (0.02 mag at J) is obtained by including another period, e.g. 275 d, but more data are required to establish the reality of this.

L_2 Pup (not illustrated). This seems to have a period of 137 d and a highly variable amplitude. This could be an example of a star with two very similar periods which appears to have a very low amplitude when the two destructively interfere. A residual of 0.11 mag at J results from fitting periods of 136.8 and 135.5 d, which is an improvement over the 0.15 mag residual resulting from the 137-d fit. Nevertheless a much longer time-base of good quality observation is the only way to examine for such periodicity.

UU Tuc. The main period is at $P = 326$ d, but the illustrated curve in Fig. 27 shows the additional contributions from $2P$ and a long term trend. The evidence for the $2P$ contribution is inconclusive; if it is present then the star has alternating deep and shallow minima, otherwise it has highly variable minima. The residuals from the illustrated curve are 0.12 and 0.09 mag at J and L respectively.

10 CONCLUSIONS

The period–colour relationships for Mira-like variables with minimal dust shells were derived and discussed. It was shown that the colour, at a particular period, depends on the pulsation amplitude of the star, presumably because stars with large amplitudes have very extended atmospheres and therefore different colours from their low-amplitude counterparts. Stars with extended atmospheres also have higher mass-loss rates, as one would anticipate if mass-loss were driven by pulsation.

Two sequences were identified in the $Hp - K$ versus $\log P$ diagram. At a given period the two groups have similar amplitudes but different spectral types and infrared colours. The short period stars in the bluer group have similar colours to the Miras found in globular clusters. These groups are discussed in more detail in Papers II and III.

ACKNOWLEDGMENTS

We are particularly grateful to Boris Yudin for allowing us to use his IR observations from the Crimea observatory and to Stefano Bagnulo, Ian Short and Tom Lloyd Evans for allowing us to use their SAAO *JHKL* photometry in advance of publication. We thank the following people for their contribution to the SAAO observations reported here: Brian Carter, Robin Catchpole, Ian Glass, Dave Laney, Karen Pollard, Greg Roberts, Jonathan Spencer-Jones, Garry Van Vuran, Hartmut Winkler and Albert Zijlstra. We also thank Luis Balona for the use of his STAR Fourier analysis package. This paper is based on data from the *Hipparcos* astrometry satellite and from the South African Astronomical Observatory.

REFERENCES

Barnes T. G., 1973, ApJS, 25, 369
Barthès D., Mattei J. A., 1997, AJ, 113, 373
Bateson F., McIntosh R., Venimore C. W., 1988, R. Astron. Soc. New Zealand Publ. Var. Star Sec., 15, 70
Bedding T. R., Conn B. C., Zijlstra A. A., 2000, in Szabados L., Kurtz D. W., eds, ASP Conf. Ser. Vol. 203, The Impact of Large-Scale Surveys on Pulsating Star Research. Astron. Soc. Pac., San Francisco, p. 96
Bessell M. S., Brett J. M., Scholz M., Wood P. R., 1989, A&A, 213, 209
Campbell L., 1955, Studies of Long Period Variables. AAVSO, Massachusetts
Carter B. S. C., 1990, MNRAS, 242, 1
Catchpole R. M., Robertson B. S. C., Lloyd Evans T. H. H., Feast M. W., Glass I. S., Carter B. S., 1979, SAAO Circ., 1, 61
Feast M. W., 1980, in Iben A., Renzini A., eds, Physical Processes in Red Giants. Reidel, p. 193
Feast M. W., 1996, MNRAS, 278, 11
Feast M. W., Whitelock P. A., 1999, in Caputo F., Heck A., eds, Post-*Hipparcos* Candles. Heck, Kluwer, Dordrecht, p. 75
Feast M. W., Whitelock P. A., 2000, in Giovannelli F., Matteucci F., eds, The Chemical Evolution of the Milky Way. Kluwer, in press
Feast M. W., Whitelock P. A., 2000b, MNRAS, 317, 460 (Paper III)
Feast M. W., Robertson B. S. C., Catchpole R. M., Lloyd Evans T., Glass I. S., Carter B. S., 1982, MNRAS, 201, 439
Feast M. W., Glass I. S., Whitelock P. A., Catchpole R. M., 1989, MNRAS, 241, 375
Feast M. W., Whitelock P. A., Carter B. S., 1990, MNRAS, 247, 227
Gezari D. Y., Pitts P. S., Schmitz M., 1997, Catalog of Infrared Observations, Edition 4, unpublished
Glass I. S., Whitelock P. A., Catchpole R. M., Feast M. W., 1995, MNRAS, 273, 383
Groenewegen M. A. T., de Jong T., 1998, A&A, 337, 797
Hron J., 1991, A&A, 252, 583
IRAS Science Team, 1988, Explanatory Supplement to the IRAS Point Source Catalogue, NASA
Keenan P. C., Garrison R. F., Deutsch A. J., 1974, ApJS, 28, 271
Kholopov P. N. et al., 1985, General Catalogue of Variable Stars 4th edn. Nauka Publishing House, Moscow (GCVS)
Koen C., Lombard F., 1995, MNRAS, 274, 821
Le Bertre T., Winters J. M., 1998, A&A, 334, 173
Lloyd Evans T., 1985a, in Jaschek M., Keenan P. C., eds, Cool Stars with Excess of Heavy Elements. Reidel, p. 163
Lloyd Evans T., 1997, MNRAS, 286, 839
Lloyd Evans T., Menzies J. W., 1973a, in Fernce J. D., eds, Variable Stars in Globular Clusters and Related Systems. Reidel, p. 151
Lysacht M. G., 1989a, J. AAVSO, 18, 10
Lysacht M. G., 1989b, J. AAVSO, 18, 17
Lysacht M. G., 1989c, J. AAVSO, 18, 28
Mattei J. A., 1983, AAVSO Report 38
Mattei J. A., 1997, J. AAVSO, 25, 57
Mattei J. A., Foster G., Hurwitz L. A., Malatesta K. H., Willson L.-A., Mennessier M. O., 1997a, in Battrick B., eds, *Hipparcos* - Venice '97', ESA SP-402
Mennessier M. O., Boughaleb H., Mattei J. A., 1997, A&AS, 124, 143
Menzies J. W., Whitelock P. A., 1985, MNRAS, 212, 783
Moshir M. et al., 1989, IRAS Faint Source Catalog, Version 2. Infrared Processing and Analysis Centre, ESO
Payne-Gaposchkin C., 1954, Variable Stars and Galactic Structure. Athlone Press, London
Percy J. R., Bagby D. H., 1999, PASP, 111, 203
Percy J. R., Colivas T., 1999, PASP, 111, 94
Perryman M. A. C. et al., 1997, The *Hipparcos* and Tycho Catalogues, ESA SP-1200
Robertson B. S. C., Feast M. W., 1981, MNRAS, 196, 111
Walker W. S. G., Ives F. V., Williams H. O., 1995, Southern Stars, 36, 123
Whitelock P. A., 1987, PASP, 99, 573
Whitelock P. A., 1997a, in Ferlet R., Maillard J.-P., Raban B., eds, Variable Stars and the Astrophysical Returns of Microlensing Surveys. Editions Frontieres, Gif-Sur-Yvette
Whitelock P. A., 1999, in Takeuri M., Sasselor D., eds, Pulsating Stars –

Recent Developments in Theory and Observation. Universal Academy Press, Tokyo, p. 31
Whitelock P. A., 2000, in Wing R., eds, IAU Symp. 177, The Carbon Star Phenomenon. Kluwer, Dordrecht, p. 179
Whitelock P. A., Feast M. W., 2000, MNRAS, 319, 759 (Paper II, this issue)
Whitelock P. A., Pottasch S. R., Feast M. W., 1987b, in Kwok S., Pottasch S. R., eds, Late Stages of Stellar Evolution. Reidel, Dordrecht, p. 269
Whitelock P. A., Menzies J. W., Feast M. W., Marang F., Carter B., Roberts G., Catchpole R. M., Chapman J., 1994, MNRAS, 267, 711
Whitelock P. A., Feast M. W., Marang F., Overbeek M. D., 1997, MNRAS, 288, 512

This paper has been typeset from a TEX/LATEX file prepared by the author.